18

LIGHT SCATTERING AND ITS APPLICATIONS IN POLYMER CHARACTERIZATION

Roberto Alexander-Katz

18.1 INTRODUCTION

Electromagnetic scattering phenomena occur when an electromagnetic field interacts with a medium that is heterogeneous at a scale of the wavelength of the incident field; that is, a material might look perfectly homogenous to the eye, however, when a laser beam goes across it, light will scatter in all directions other than those given by the refraction and reflection laws. Examples of this can be found in simple liquids such as highly clarified benzene or carbon disulfide, where density fluctuations at the scale of the wavelength of visible light give rise to scattering that is observable by the naked eye. In the case of polymer solutions or particle suspensions, the local fluctuations in the dielectric constant take place due to fluctuations in local concentration as well as the density fluctuations. The analysis of such fluctuations gave rise to two popular applications of this technique: the determination of molecular weights and sizes of macromolecules by static light scattering (SLS) and particle sizing by dynamic light scattering (DLS). However, light scattering together with its sister techniques, namely, small-angle X-ray scattering (SAXS), small-angle neutron scattering (SANS), and inelastic neutron scattering (INS), can give more information about the structure of the scattering objects, the thermodynamics, and the dynamic processes taking place in complex systems.

In this chapter, we emphasize on the principles in which light scattering methods are founded and apply these to different systems. We also stress the importance of a solid theoretical framework in the field of polymers or other complex systems in expanding the scope of applications of these tools beyond the standard applications.

Unfortunately, because of space, we have not covered important new developments in light scattering for the study of nontransparent systems such as diffusion wave spectroscopy (DWS), fiber-optic quasi-elastic light scattering (FOQELS), dual-color cross-correlation, 3D cross-correlation DLS, and improved techniques followed from these techniques [1–4].

In the first section, we introduce the general theory of light scattering. The second section is devoted to SLS, and we give some examples of its application. In the third section, we discuss the principles of DLS and we apply these to the study of the dynamics of different systems, whether dilute or concentrated solutions.

18.2 PRINCIPLES OF STATIC AND DYNAMIC LIGHT SCATTERING

Let us consider an electromagnetic field incident on a small volume element on the order of λ^3, where λ is the wavelength of light in the material (solution, particle suspension, etc.); due to the imbalance of the molecules that enter and leave such volume, there will be fluctuations in density, concentration, and others that concomitantly will produce fluctuations in the local dielectric constant. Let us denote by $\Delta\varepsilon(\mathbf{R}, t)$ the deviation of the dielectric constant from its mean $\langle\varepsilon\rangle$ at $\mathbf{R}$ and time t. Since these

Handbook of Polymer Synthesis, Characterization, and Processing, First Edition. Edited by Enrique Saldívar-Guerra and Eduardo Vivaldo-Lima.

fluctuations are in most cases very small, we can assume that the scattered electric field E_s will be proportional to $\Delta\varepsilon$ and to the incident electric field E_0; that is,

$$E_s \approx \Delta\varepsilon(\mathbf{R}, t)E_0 \tag{18.1}$$

However, in the scattering volume *V,* there are a great number of volume elements that contribute to the total scattered electric field. If $\Delta\varepsilon(\mathbf{R}, t)$ is very small, we can consider that each molecule in V is sensing the same incident field, and therefore, we can write the scattering field just as a superposition of the fields coming from all elements of our scattering volume. This approximation is called the *Rayleigh-Debye-Gans approximation* (*RDGA*) and is valid when $\Delta\varepsilon \ll 1$ and the phase shifts induced by the fluctuations are very small [5]. This is the case of any simple fluid or solution away from its critical point (or critical line). However, there are cases where these conditions are not met, such as a suspension of latex particles where the refractive index of the particles differs substantially from that of the suspending fluid. In the latter case, the internal field at any point in the domain is not the same as the applied field, and one has to consider the contribution of all elements in the domain. There are a several approaches to this end, some analytical, such as Mie's theory for spheres and cylinders, and others numerical for particles with no particular symmetries, such as the T-matrix theory [6, 7]. However, for most of the classical light scattering applications to polymer characterization in solution, the RDGA is fully satisfied, and therefore, we discuss it thoroughly in what follows. In any case, we will point out along the chapter whenever a Mie-type calculation is required.

The measured quantity is the intensity of the scattered field, that is, the square of the scattered field,

$$I_s = E_s \cdot E_s^* \tag{18.2}$$

Therefore, the total scattered intensity will be the sum of the cross products of the scattered electric fields from different volume elements. Yet, these fields can interfere between each other in view that they might be out of phase, due to the difference in optical paths, and the motion of the molecules can induce frequency changes. This leads finally to an expression for the scattered intensity

$$I_s(\mathbf{q}, \Delta\omega) \approx I_0 \iint \left\langle \Delta\varepsilon(\mathbf{R}, t)\Delta\varepsilon^*(\mathbf{R}', 0)\right\rangle \exp\left(-i\left[\mathbf{q}(\mathbf{R} - R') + \left(\omega - \omega_0\right)t\right]\right) \mathrm{d}\mathbf{R}\mathrm{d}\mathbf{R}'\mathrm{d}t \tag{18.3}$$

where I_0 is the incident intensity and

$$\mathbf{q} = \mathbf{k} - \mathbf{k}' \tag{18.4}$$

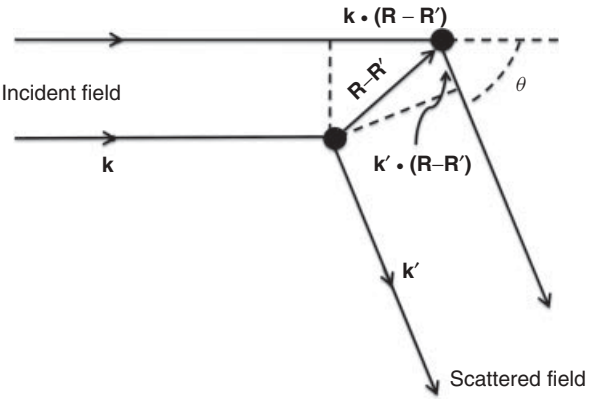

Figure 18.1 Schematics of the changes in optical paths.

while $\mathbf{k}$ and $\mathbf{k}'$ are the wave vectors of the incident and scattered fields, respectively, as shown in Figure 18.1. From this figure, it can be seen that $\mathbf{q}\cdot(\mathbf{R}\text{-}\mathbf{R}')$ corresponds to the difference in optical paths between the fields that are scattered by two molecules that are $\mathbf{R} - \mathbf{R}'$ apart. We have added average brackets to the product of the local dielectric constant differences (dielectric constant correlation function) since these are varying randomly, and therefore, we only observe an average in a typical measurement.

A formal derivation of Equation 18.3 leads to [8]

$$I_s(\mathbf{q}, \Delta\omega) = \frac{I_0 V k^4 \sin^2\alpha}{32\pi^3\varepsilon_0^2 r^2} \iint \left\langle \Delta\varepsilon(\mathbf{R}, t)\Delta\varepsilon^*(0, 0)\right\rangle \exp\left(-i\left[\mathbf{q}\cdot\mathbf{R} + \Delta\omega t\right]\right) \mathrm{d}\mathbf{R}\mathrm{d}t \tag{18.5}$$

where it has been made use of translational invariance; k is the wavenumber $(2\pi/\lambda)$ in the medium, ε_0 is the vacuum dielectric constant, r is the distance from the scattering volume to the observer, and α is the angle of observation relative to the linearly polarized incident field, as shown in Figure 18.2. The r dependence arises because any element of the scattering volume is a source of spherical waves, and the irradiance of a point source decays as $1/r^2$. The $\sin^2\alpha$ factor comes from the transversal nature of the electromagnetic waves; that is, for a vertically polarized incident beam, the only component of the field that will propagate in the direction shown in Figure 18.2 will be $\approx \sin\alpha$, and therefore, the scattered intensity will be $\approx \sin^2\alpha$. Finally, Rayleigh has shown that the light scattered by any small volume element (as compared to λ) should scale as $1/\lambda^4 \approx k^4$ [9]. All these front factors are related to the instrument and not to the optical properties of the sample. For a given instrument, we will only vary the scattering angle θ.

If the detecting system does not have any device that can resolve the frequency (or time) dependence of I_s, such as

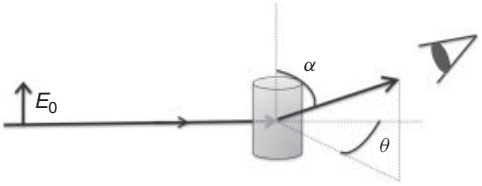

Figure 18.2 Scattering geometry.

a correlator, Fabry–Perot interferometer, or, as discussed later, if the setup of the detecting system is not appropriate to observe the intensity fluctuations with time, then this will be equivalent to integrating over all frequencies, and Equation 18.5 reduces to

$$I_s(\mathbf{q}) = \frac{I_0 V k^4 \sin^2\alpha}{16\pi^2\varepsilon_0^2 r^2}\int \left\langle \Delta\varepsilon(\mathbf{R})\Delta\varepsilon^*(\mathbf{0})\right\rangle \exp(-i\mathbf{q}\cdot\mathbf{R})\,d\mathbf{R} \tag{18.6}$$

In this case, we will be speaking of SLS since time is not involved any more. Equation 18.6 actually represents the point of departure of the classical light scattering applications: the determination of molecular weights and radius of gyration of polymer molecules. Since

$$|\mathbf{q}| = \frac{4\pi}{\lambda}\sin\frac{\theta}{2} \tag{18.7}$$

this means that varying the angle is equivalent to changing the wavelength. This fact makes scattering a unique technique because we can change the scale of our probe (wavelength) by simply observing our sample at a different angle. As we approach the incoming beam, θ becomes very small, and this is equivalent to having a large effective wavelength of

$$\lambda_{\text{eff}} = \frac{\lambda}{\sin(\theta/2)} \tag{18.8}$$

If instead of light we use an X-ray source, the only difference from the previous discussion is that we will substitute the fluctuations in the dielectric constant by the fluctuations in the electronic density. X-ray wavelength is typically on the order of 1.5 Å. However, if we perform SAXS at angles of the order of 2 min from the incoming beam, it would be equivalent to change the scale of our probe by more than 3400 times! This means that using the *same* wavelength, the scale of our probe can change from 1.5 to 5100 Å, overlapping the visible region of the electromagnetic spectrum. This allows us to explore our material in a wide range of scales without having absorption effects, as is the case with spectroscopic techniques. All this can be extended to neutron sources with the difference that instead of electron clouds, neutrons interact with the nucleus of the atoms and the magnetic fields of their impaired electrons. Thermal neutron sources have equivalent wavelength as X-rays, and therefore, neutron scattering at small angles (SANS) is a powerful tool to explore condensed matter in a wide range of scales. Neutrons, X-rays, and light scattering are complementary techniques very much used in the study of polymers in solution or in solid state [10, 11].

Since both Equations 18.5 and 18.6 depend on instrumental variables, it is customary to introduce the so-called Rayleigh ratio R_θ, so that the results are independent of the geometry and intensity of the light source used; that is,

$$R_\theta = I_s(\mathbf{q})\frac{r^2}{V I_0 \sin^2\alpha} = \frac{k^4}{16\pi^2\varepsilon_0^2}\int \left\langle \Delta\varepsilon(\mathbf{R})\Delta\varepsilon^*(\mathbf{0})\right\rangle \exp(-i\mathbf{q}\cdot\mathbf{R})d\mathbf{R} \tag{18.9}$$

In Equation 18.9, we observe two competing factors: $\langle\Delta\varepsilon(\mathbf{R})\Delta\varepsilon^*(\mathbf{0})\rangle$ and the interference factor $\exp(-i\mathbf{q}\cdot\mathbf{R})$. The dielectric constant correlation function will tend to be zero for distances greater than the correlation length ξ. For dilute systems, this length is related to a characteristic length of the heterogeneities in the system, such as the particle size or the radius of gyration of a macromolecule. On the other hand, $|\mathbf{q}|^{-1}$ is proportional to the effective scale ($\lambda/\sin(\theta/2)$) with which we are probing our system. The ratio between these two lengths defines differences between the theoretical approaches for the calculation of Equation 18.9. In the limiting case of $q^{-1}/\xi \gg 1$ that corresponds to $\theta \to 0$, the particles or macromolecules will appear as points without structure since the scale of observation is much larger than their own size, as shown schematically in Figure 18.3. We will call this as the *thermodynamic limit* because the excess of light scattered is due to the imbalance between the incoming and exit of the macromolecules or particles *as a whole* in a volume element of the order of q^{-3}, that is, due to the local fluctuations in the number of molecules in the system, which is a thermodynamic variable.

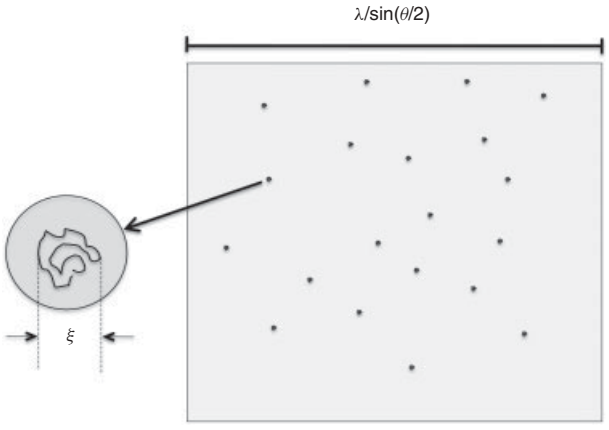

Figure 18.3 Small-angle limit. In this limit, all macromolecules appear as point particles compared to the volume probed.

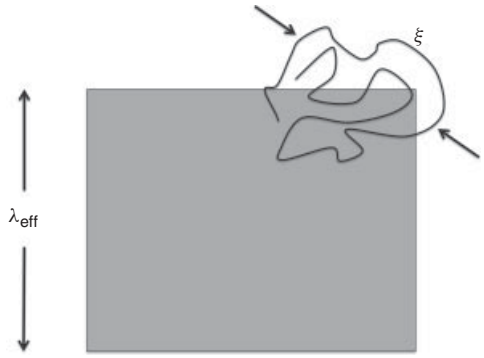

Figure 18.4 When ξ is of the order of magnitude of or greater than the effective wavelength, the *partial* entrance of the macromolecule or particle will produce fluctuations in the scattered intensity.

On the other hand, if $q^{-1} \approx \xi$, the excess in the fluctuations is due to the imbalance between the entrance and exit of a *fraction* of a macromolecule (or particle) as shown schematically in Figure 18.4. The latter is not a thermodynamic variable, and for these values of q, the scattering will be sensitive to the *structure* of the macromolecule.

In the next two sections, we discuss the SLS by dilute polymer solutions in both cases: in the limit of small angles and when q^{-1} is of the order or smaller than ξ.

18.3 STATIC LIGHT SCATTERING BY DILUTE POLYMER SOLUTIONS

18.3.1 Scattering at Small Angles ($q\xi \ll 1$): Determination of Molecular Weights and Thermodynamic Properties

As shown schematically in Figure 18.3, in the limit of small angles, the effective volume that we are probing is very large in comparison with the volume occupied by a single macromolecule (or particle). Therefore, the number of polymer molecules within this volume is considerably large. As we approach $\theta \approx 0$, this scale becomes quasi-macroscopic, and we can reduce the calculation of the fluctuations in the dielectric constant to that of the fluctuation of the thermodynamic degrees of freedom of the system. In fact, in the limit where $q^{-1} \gg \xi$, $\langle \Delta\varepsilon(\mathbf{R})\Delta\varepsilon(0)\rangle = \langle(\Delta\varepsilon)^2\rangle\,\delta(\mathbf{R})$, where $\langle(\Delta\varepsilon)^2\rangle$ is the thermodynamic fluctuation in the dielectric constant. In addition, since $|\, q\,\xi\,| \ll 1$, $\exp(-i\,q\,\xi) \approx 1$. Hence, when $\theta \to 0$, Equation 18.9 can be approximated by

$$R_\theta = \frac{k^4 V}{16\pi^2 \varepsilon_o^2} \left\langle (\Delta\varepsilon)^2 \right\rangle \tag{18.10}$$

The theory of thermodynamic fluctuations in the context of light scattering was introduced first by Smoluchowski and Einstein [12, 13]. Einstein considered that the scattering of light in a solution arises from local density and concentration fluctuations. However, it was only till the late 40s and early 50s that Brinkman and Hermans [14], Stockmayer [15], and Kirkwood and Goldberg [16] adopted this approach in the context of light scattering by polymer solutions. Here, we summarize only the basic results for a binary mixture.

In a binary mixture, there are 3 degrees of freedom and it can be proved that the fluctuations in the dielectric constant can be reduced to the sum of the fluctuation in the density of the pure solvent plus the fluctuations in the molar concentration of macromolecules,

$$\left\langle (\Delta\varepsilon)^2 \right\rangle = \left(\frac{\partial\varepsilon}{\partial\rho_s}\right)^2 \left\langle (\Delta\rho_s)^2 \right\rangle + \left(\frac{\partial\varepsilon}{\partial N_1}\right)^2 \left\langle (\Delta N_1)^2 \right\rangle \tag{18.11}$$

where ρ_s is the density of the pure solvent and N_1 is the number of moles of the solute. However, the first term corresponds to the contribution of the light scattered by the solvent and can be measured independently. Therefore, if we subtract this term from $\langle(\Delta\varepsilon)^2\rangle$, we will obtain the excess in the fluctuation in the dielectric constant due to the fluctuation in concentration of the solute, that is,

$$\left\langle (\Delta\varepsilon)^2 \right\rangle_{ex} = \left(\frac{\partial\varepsilon}{\partial N_1}\right)^2 \left\langle (\Delta N_1)^2 \right\rangle = \left(\frac{\partial\varepsilon}{\partial N_1}\right)^2 \frac{k_B T}{\left(\partial\mu_1/\partial N_1\right)_{TP}} \tag{18.12}$$

where μ_1 is the chemical potential of the solute and k_B is the Boltzmann constant. If we write this expression in terms of the solute weight concentration c_1 (in g/cc), then

$$\begin{aligned} \left\langle (\Delta\varepsilon)^2 \right\rangle_{ex} &= \frac{M_1}{N_A V} \left(\frac{\partial\varepsilon}{\partial c_1}\right)^2 \frac{k_B T}{\left(\partial\mu_1/\partial c_1\right)_{TP}} \\ &= \frac{k_B T c_1}{N_0 V_0} \left(\frac{\partial\varepsilon}{\partial c_1}\right)^2 \frac{1}{\left(\partial\pi/\partial c_1\right)_{TP}} \end{aligned} \tag{18.13}$$

where N_0 is the number of moles of the solvent, V_0 is the molar volume of the solvent, and π is the osmotic pressure. Hence, the excess Rayleigh factor will be

$$R_\theta^{ex} = \frac{k^4 k_B T c_1}{16\pi^2 \varepsilon_0^2} \left(\frac{\partial\varepsilon}{\partial c_1}\right)^2 \frac{1}{\left(\partial\pi/\partial c_1\right)_{TP}} \tag{18.14}$$

where we have made the approximation $N_0 V_0 \approx V$ since we are in the limit of dilute solution. Equation 18.14 establishes a relation between light scattering and the osmotic pressure, valid in the limit $\theta \to 0$. This relation constitutes the basis for the determination of the molecular weight and other thermodynamic properties by light scattering.

Using the virial expansion for the osmotic pressure, we can write π as

$$\pi = \mathrm{RT}c_1\left(\frac{1}{M} + A_2c_1 + A_3c_1^2 + \cdots\right) \tag{18.15}$$

where A_2, A_3, ... are the virial coefficients. Then,

$$R_\theta^{\mathrm{ex}} = \frac{k^4c_1}{16\pi^2\varepsilon_0^2}\left(\frac{\partial\varepsilon}{\partial c_1}\right)^2\frac{1}{N_\mathrm{A}\left({}^1\!/_M + 2A_2c_1 + \cdots\right)} \tag{18.16}$$

It is common to regroup all constants into one constant as[1]

$$K = \frac{4\pi^2}{\lambda^4N_\mathrm{A}}\left[n_0\left(\frac{\partial n}{\partial c_1}\right)\right]^2 \tag{18.17}$$

where n and n_0 are the refractive indexes of the solution and the solvent, respectively, and we have used the relation $n = \sqrt{(\varepsilon/\varepsilon_0)}$. Equation 18.16 then takes the form

$$\frac{Kc_1}{R_\theta^{\mathrm{ex}}} = \frac{1}{M} + 2A_2c_1 + 3A_3c_1^2 + \cdots \tag{18.18}$$

The generalization of Equation 18.18 to polydisperse homopolymers is

$$\frac{Kc}{R_\theta^{\mathrm{ex}}} = \frac{1}{\langle M\rangle_\mathrm{w}} + 2\langle A_2\rangle_\mathrm{w}c + \cdots \tag{18.19}$$

where c is the polymer concentration (in g/cc) and $\langle M\rangle_\mathrm{w}$ and $\langle A_2\rangle_\mathrm{w}$ are given by

$$\langle M\rangle_\mathrm{w} = \sum_i M_iw_i \tag{18.20}$$

and

$$\langle A_2\rangle_\mathrm{w} = \frac{1}{\langle M\rangle_\mathrm{w}^2}\sum_i\sum_j M_iM_jA_{ij}w_iw_j \tag{18.21}$$

where w_i and M_i are the weight fraction and molecular weight of species i, respectively. The difference between a direct determination of the molecular weight by osmometry and that with light scattering is that they average differently. The former averages number wise while the latter does it by weight. This also applies to the virial coefficients. Furthermore, in Equation 18.16, there is a front factor $(\partial\varepsilon/\partial c_i)^2$ for each species, which in the case of homopolymers are the same, independently of molecular weight, and can be factored out as in Equation 18.19. However, if the species in question differ also in composition, the $(\partial\varepsilon/\partial c_i)^2$ term will be different for each species and cannot be factored out, giving rise to an apparent molecular weight as in the case of copolymers. The same occurs when we have a solution of mixed solvents and a homopolymer; again the extrapolation at $c \to 0$ and $\theta \to 0$ will give rise to an apparent molecular weight because of the preferential sorption of each solvent component in the polymer molecule [17]. In these cases, different authors have proposed alternative methodologies to determine the weight-average molecular weight [18–20]. To illustrate this, let us consider the case of copolymers. If we define the K_i as

$$K_i = K^*\left(\frac{\partial n}{\partial c_i}\right)^2\bigg|_{c=0} = K^*\nu_i^2 \tag{18.22}$$

where

$$K^* = \frac{4\pi^2n_0^2}{N_\mathrm{A}\lambda^4} \tag{18.23}$$

and

$$\nu_i = \left(\frac{\partial n}{\partial c_i}\right)\bigg|_{c=0} \tag{18.24}$$

Then,

$$\frac{K^*\nu^2c}{R_\theta^{\mathrm{ex}}}\bigg|_{\substack{c\to0\\\theta\to0}} = \frac{1}{\frac{1}{\nu^2}\sum\limits_i\frac{c_i}{c}M_i\nu_i^2} = \frac{1}{M_\mathrm{app}} \tag{18.25}$$

where c is the concentration of the copolymer in the solution and ν is the specific increment in the refractive index of the copolymer solution extrapolated to $c \to 0$. This means that if we followed the same procedure as with homopolymers, we are actually measuring a molecular weight given by

$$M_\mathrm{app} = \frac{1}{\nu^2}\sum_i\frac{c_i}{c}M_i\nu_i^2 \tag{18.26}$$

Since ν_i depends of the solvent used, the molecular weight determined in this way is necessarily apparent.

If we assume that the specific refractive index increments follow a weight sum rule, then for copolymers made of two monomers A and B, the relationship between M_app and $\langle M\rangle_\mathrm{w}$ can be expressed as

$$M_\mathrm{app} = \left(\frac{\nu_\mathrm{A}\nu_\mathrm{B}}{\nu^2}\right)\langle M\rangle_\mathrm{w} + \left[\frac{\nu_\mathrm{A}\left(\nu_\mathrm{A}-\nu_\mathrm{B}\right)}{\nu^2}\right]W\langle M_\mathrm{A}\rangle_\mathrm{w} + \left[\frac{\nu_\mathrm{B}\left(\nu_\mathrm{B}-\nu_\mathrm{A}\right)}{\nu^2}\right](1-W)\langle M_\mathrm{B}\rangle_\mathrm{w} \tag{18.27a}$$

[1]This expression for K is valid for vertically polarized light. In what follows in this chapter, we assume that the incident field is vertically polarized and that we are observing in the plane of incidence, that is, $\sin\alpha = 1$. For light that is polarized horizontally, Equation 18.17 should have a factor $\cos^2\theta$, and for unpolarized light, the factor should be $(1 + \cos^2\theta)/2$.

$\langle M_A \rangle_w$ and $\langle M_B \rangle_w$ being the weight averages of the components A and B of the copolymer, respectively, while ν_A and ν_B are the specific refractive index increments of the solution with homopolymer types A and B, respectively. W is the average weight fraction of A in the copolymer. The relationship can alternatively be expressed as

$$M_{app} = \langle M \rangle_w + 2P\left(\frac{\nu_A - \nu_B}{\nu}\right) + Q\left(\frac{\nu_A - \nu_B}{\nu}\right)^2 \tag{18.27b}$$

P and Q are given by

$$P = \sum_i \frac{c_i}{c} M_i \delta W_i \tag{18.28}$$

$$Q = \sum_i \frac{c_i}{c} M_i \left(\delta W_i\right)^2 \tag{18.29}$$

with $\delta W_i = W_i - W$, where W_i is the weight fraction of monomer A in the copolymer of the species i.

According to Equation 18.27b, the molecular weight measured depends on $\langle M \rangle_w$ as well as on the first two moments of the distribution in composition. In principle, by index matching with a single solvent, we could obtain $\langle M \rangle_w$, $\langle M_A \rangle_w$, $\langle M_B \rangle_w$, and Q.

A common procedure to determine $\langle M \rangle_w$ is to perform several light scattering experiments to measure M_{app} with different solvents with a reasonably range of values of $(\nu_A - \nu_B)/\nu$ and finally obtain by regression methods the parameters of the parabola in Equation 18.27b. The latter procedure will provide not only $\langle M \rangle_w$ but also P and Q, which give us information about the first two moments of the distribution in composition. However, to have a reasonable accuracy, at least ν_A or ν_B should be large in order to increase the overall intensity of the scattered light. Unfortunately, it is difficult to find a one-component solvent to index match or fulfill the requirements of the regression method. Therefore, we are forced to use mixed solvents, which in turn will add an extra complication due to preferential sorption. Casassa and Eisenberg have shown that in the case of mixed solvents, we can use one-component solvent light scattering relationships if we substitute the conventional refractive index increment measured at constant composition of the mixed solvents by ν's measured at constant chemical potential (ν_μ) for all diffusible components of the solvent, that is, after the establishment of osmotic equilibrium between the polymer solution and the polymer-free mixed solvents [21, 22]. The experimental procedures to determine ν_μ's are described by Tuzar et al. [23, 24]. A thorough test of the Bushuk–Benoit theory was conducted by Podešva et al. [25].

On the other hand, since, in the case of mixed solvent, light scattering is sensitive to preferential sorption by polymers, it has been used as a tool in the study of such important phenomena [26–33]. An elegant example of the study of preferential sorption by light scattering is that of Marchal and Strazielle who studied the thermal transitions from coil to helix of poly(L-benzyl glutamate) in a mixture of dichloro acetic acid (DCA) and heptane; they found an unusual variation in the apparent molecular weight (Fig. 18.5) as the conformation changed from coil to helix, indicating that the helical structure adsorbed fewer DCA molecules than the coiled form [32].

Finally, as per Equation 18.27b, if a copolymer has a very narrow composition distribution, M_{app} will be very close to $\langle M \rangle_w$ using a single solvent; the same applies to mixed solvents if we follow the procedure mentioned earlier. This can be the case, for instance, of a radical copolymerization in a true azeotrope composition or of a block copolymer synthesized by a controlled anionic or living radical polymerization.

18.3.2 Application of SLS for the Determination of Structure When $|q\,\xi| \geq 1$

In this section, we discuss the application of the RDGA for arbitrary q's. When the scale with which we are probing our system is on the order of the radius of gyration of our macromolecule (Fig. 18.4), the calculation of $\langle \Delta\varepsilon(\mathbf{R})\Delta\varepsilon(\mathbf{0})\rangle$ will not reduce to the thermodynamic fluctuations since the number of monomers in a volume element is not a thermodynamic variable and, additionally, in this case, $\exp(-i\,\mathbf{q}\cdot\mathbf{R})$ is an oscillating function in the probing volume element.

However, we can still follow the steps from the previous section if we assume that the dielectric constant depends on $\mathbf{R}$ through the local volume fraction occupied by the solvent $\varphi(\mathbf{R})$, the number of monomers in that volume element $N_1(\mathbf{R})$, and the local temperature $T(\mathbf{R})$, that is,

$$\varepsilon(\mathbf{R}) = \varepsilon\left[\varphi(\mathbf{R}), N_1(\mathbf{R}), T(\mathbf{R})\right] \tag{18.30}$$

Here, $\varphi(\mathbf{R})$ and $T(\mathbf{R})$ are the thermodynamic variables, while $N_1(\mathbf{R})$ is not. However, we can still assume that $N_1(\mathbf{R})$ is not correlated with $\varphi(\mathbf{R})$ and $T(\mathbf{R})$ and thus calculate the excess in the fluctuations in the dielectric constant as

$$\left\langle \Delta\varepsilon\,(\mathbf{R})\,\Delta\varepsilon\left(\mathbf{R}'\right)\right\rangle_{ex} = \left(\frac{\partial\varepsilon}{\partial N_1}\right)^2 \left\langle \Delta N_1\,(\mathbf{R})\,\Delta N_1\left(\mathbf{R}'\right)\right\rangle \tag{18.31}$$

We can write Equation 18.31 in terms of the number density of monomers $\rho_1 = N_1/V$ as

$$\left\langle \Delta\varepsilon\,(\mathbf{R})\,\Delta\varepsilon\left(\mathbf{R}'\right)\right\rangle_{ex} = \left(\frac{\partial\varepsilon}{\partial\rho_1}\right)^2 \left\langle \Delta\rho_1\,(\mathbf{R})\,\Delta\rho_1\left(\mathbf{R}'\right)\right\rangle \tag{18.32}$$

The Fourier transform of correlation function of the local number densities of monomers can be written in terms of

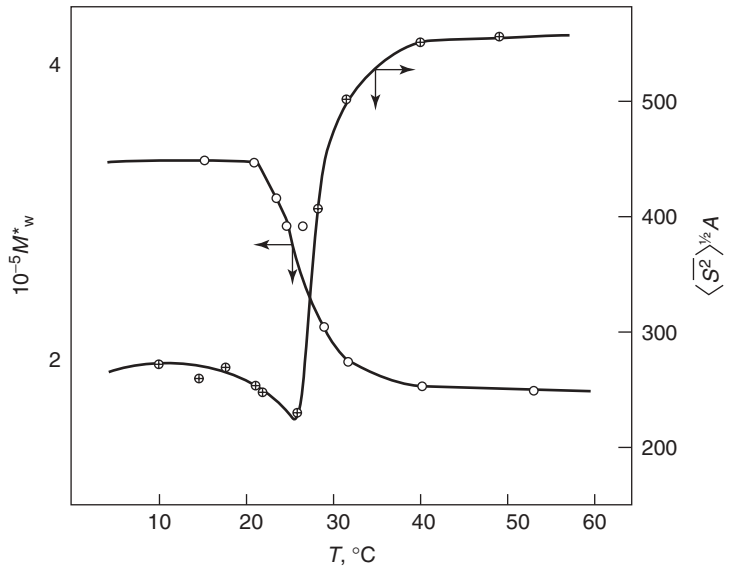

Figure 18.5 Helix–coil transitions of poly(L-benzyl glutamate) in a mixture of dichloroacetic acid and heptane showing the variation of the apparent molecular weight (M^*_w in their notation) and the radius of gyration. *Source*: Reprinted with permission from Cowie JMG. *Pure Appl Chem* 1970;23:355 [33]. Copyright 1970 International Union of Pure and Applied Chemistry (after Marchal E, Strazielle C. *Compt Rendu* 1968;C267:135. Academie Française de Science).

$G(\mathbf{R}, c)$, the joint probability of finding any monomer at $\mathbf{R}$ when any other is at the origin, as

$$\iint \left\langle \Delta\rho_1(\mathbf{R})\, \Delta\rho_1\left(\mathbf{R}'\right)\right\rangle \exp\left(-i\mathbf{q}\left[\mathbf{R}-\mathbf{R}'\right]\right) \mathrm{d}\mathbf{R}\mathrm{d}\mathbf{R}' = nN_\mathrm{p}\int \left(G(\mathbf{R}, c) - \langle\rho_1\rangle\right) \exp\left(-i\mathbf{q}\cdot\mathbf{R}\right) \mathrm{d}\mathbf{R} \quad (18.33)$$

where n is the number of monomers per chain, N_p is the number of polymer chains, and $\langle\rho_1\rangle$ is the average number density of monomers. We have explicitly written the dependence of $G(\mathbf{R}, c)$ on polymer concentration because the average $\left\langle\Delta\rho_1(\mathbf{R})\Delta\rho_1(\mathbf{R}')\right\rangle$ depends on the actual polymer concentration. It is common to divide $G(\mathbf{R}, c)$ in terms of the intramolecular and the intermolecular contributions, $G_\mathrm{intra}(\mathbf{R}, c)$ and $G_\mathrm{inter}(\mathbf{R}, c)$, respectively, as

$$G(\mathbf{R}, c) = G_\mathrm{intra}(\mathbf{R}, c) + G_\mathrm{inter}(\mathbf{R}, c) \quad (18.34)$$

where $G_\mathrm{intra}(\mathbf{R}, c)$ is the joint probability of finding any monomer at $\mathbf{R}$ when any other of the *same* macromolecule is at the origin, while $G_\mathrm{inter}(\mathbf{R}, c)$ is the joint probability of finding any monomer at $\mathbf{R}$ when any monomer of a *different* macromolecule is at the origin.

Substituting Equations 18.32, 18.33 and 18.34 into Equation 18.9, we obtain a generalization of the Rayleigh ratio of a monodisperse sample for an arbitrary q and polymer concentration as

$$\frac{R^\mathrm{ex}_\theta}{Kc} = M\left\{\frac{1}{n}\int G_\mathrm{intra}(\mathbf{R}, c)\exp\left(-i\mathbf{q}\cdot\mathbf{R}\right)\mathrm{d}\mathbf{R}\right\} + N_\mathrm{A}c\left\{\int \left(g_\mathrm{inter}(\mathbf{R}, c) - 1\right)\exp\left(-i\mathbf{q}\cdot\mathbf{R}\right)\mathrm{d}\mathbf{R}\right\} \quad (18.35)$$

where $g_\mathrm{inter}(\mathbf{R}, c) = G_\mathrm{inter}(\mathbf{R}, c)/\langle\rho_1\rangle$ and c is the concentration in g/ml of the polymer in the solution. In dilute solutions, the only relevant correlation length is related to the size of a single polymer chain, and therefore, the only surviving correlation function will be $G_\mathrm{intra}(\mathbf{R}, c)$. In the dilute limit, to first order in concentration, Equation 18.35 reduces to the well-known result [34]

$$\frac{Kc}{R^\mathrm{ex}_\theta} = \frac{1}{M\,P(\theta)} + 2A_2c + \ldots \quad (18.36)$$

where $P(\theta)$ is the normalized Fourier transform of $G_\mathrm{intra}(\mathbf{R}, c)$,

$$P(\theta) = \frac{1}{n}\int G_\mathrm{intra}(\mathbf{R})\exp\left(-i\mathbf{q}\cdot\mathbf{R}\right)\mathrm{d}\mathbf{R} \quad (18.37)$$

usually called the *form factor*. Equation 18.36 contains information on solution properties (polymer molecular weight, second virial coefficient, and so on) as well as structural information contained in $P(\theta)$, such as size

(radius of gyration), shape, and even internal structure of the macromolecule depending on how large is ξ relative to q^{-1}. In the limit of $\theta \to 0$ and $P(\theta) = 1$, Equation 18.36 reduces to Equation 18.18 for a monodisperse dilute polymer solution.

Writing $G_{\text{intra}}(\mathbf{R})$ in terms of the distribution of polymer segments $P_{ij}(\mathbf{R})$ (the probability of finding monomer j in $\mathbf{R}$ when i is at the origin), we can rewrite Equation 18.37 as

$$P(\theta) = \frac{1}{n^2} \sum_{i}^{n} \sum_{j}^{n} \int_{V} P\left(R_{ij}\right) \mathrm{e}^{-i\mathbf{q}\bullet\mathbf{R}_{ij}} \, \mathrm{d}\mathbf{R}_{ij} \tag{18.38}$$

Integrating, we arrive at the famous Debye expression for $P(\theta)$ [35]:

$$P(\theta) = \frac{1}{n^2} \sum_{i}^{n} \sum_{j}^{n} \left\langle \frac{\sin q R_{ij}}{q R_{ij}} \right\rangle \tag{18.39}$$

Debye introduced this in the context of X-ray scattering where the RDGA is commonly valid; he derived the general expression for the intensity of X-rays scattered by an ensemble of randomly oriented particles. Later on, Debye himself applied it to the scattering by polymer solutions [36, 37]. If the particle is rigid then distance between the elements that conforms to the object a_{ij} will be constant and Equation 18.39 reduces to

$$P(\theta) = \frac{1}{n^2} \sum_{i}^{n} \sum_{j}^{n} \frac{\sin q a_{ij}}{q a_{ij}} \tag{18.40}$$

This expression applies to any rigid object independent of its shape. The only assumption made was that $P_{ij}(\mathbf{R}) = P\left(R_{ij}\right)$.

Instead, we can write $P(\theta)$ in terms of the moments of the distribution polymer segments as

$$P(\theta) = \sum_{p=0}^{\infty} \frac{(-1)^p}{(2p+1)!} q^{2p} \left[\frac{1}{n^2} \sum_{i<j}^{n} \left\langle R_{ij}^{2p} \right\rangle \right] \tag{18.41}$$

If q is small compared with the inverse of the term in brackets, we can only recover up to the second moment of the distribution polymer segments, that is,

$$P(\theta) \cong 1 - \frac{1}{3} q^2 \left[\frac{1}{n^2} \sum_{i<j}^{n} \left\langle R_{ij}^2 \right\rangle \right] = 1 - \frac{1}{3} q^2 \left\langle R_{\mathrm{g}}^2 \right\rangle \tag{18.42}$$

where $\left\langle R_{\mathrm{g}}^2 \right\rangle$ is the mean square radius of gyration of the polymer chain (or particle). As q becomes larger, we can recover in addition higher moments of the distribution and therefore more information about the scattering object.

Substituting Equation 18.42 into Equation 18.36, we get in terms of the scattering angle

$$\frac{Kc}{R_\theta^{\mathrm{ex}}} = \frac{1}{M} \left[1 + \frac{16\pi^2 n_{\mathrm{s}}^2}{3\lambda^2} \left\langle R_{\mathrm{g}}^2 \right\rangle \sin^2 \left(\frac{\theta}{2} \right) + \cdots \right] + 2A_2 c + \cdots \tag{18.43}$$

where n_{s} is the refractive index of the medium.

The generalization to polydisperse polymer solutions is straightforward, leading to

$$\frac{Kc}{R_\theta^{\mathrm{ex}}} = \frac{1}{\langle M \rangle_{\mathrm{w}}} \left[1 + \frac{16\pi^2 n_{\mathrm{s}}^2}{3\lambda^2} \left\langle R_{\mathrm{g}}^2 \right\rangle_z \sin^2 \left(\frac{\theta}{2} \right) + \cdots \right] + 2 \left\langle A_2 \right\rangle_{\mathrm{w}} c + \cdots \tag{18.44}$$

where

$$\left\langle R_{\mathrm{g}}^2 \right\rangle_z = \frac{\sum_i N_i M_i^2 \left\langle R_{\mathrm{g}}^2 \right\rangle_i}{\sum_i N_i M_i^2} \tag{18.45}$$

Equation 18.44 constitutes the main expression of classical light scattering polymer characterization. This suggests the form of plotting scattering data named after Zimm [38], the *Zimm plot*, 18.37 an example of which is shown in Figure 18.6 [39]. However, there are other forms to plot scattering data depending on the form and size of the particle and the type of information that has to be extracted from the experiments. Examples of some of these will be given later in the chapter. Using either Equation 18.37 or 18.39, we can derive the form factor for different geometries, as shown in Table 18.1[2] [40].

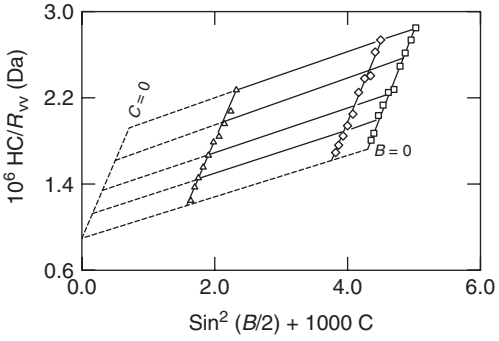

Figure 18.6 Zimm's plot of an alternating copolymer of ethylene and tetrafluoroethylene (PETFE) in diisobutyl adipate at 240 °C. *Source*: Reprinted with permission from Chu B, Wu C. *Macromolecules* 1987;20:93–98. Copyright 1987 American Chemical Society.

[2]For a sphere, the conditions of the RDGA might not be matched because the refractive index of the sphere could be substantially different from that of the suspension medium. If so, $P(\theta)$ should be calculated by Mie's theory. This is the case of PS (polystyrene) latex spheres in water.

TABLE 18.1 Form Factors for Different Geometries in the RDGA

Sphere	Rod	Gaussian Coil
$x = qa$	$x = \frac{qL}{2}$	$x = q^2\left\langle R_g^2\right\rangle$
$P(\theta) = \left[\frac{3}{x^3}(\sin x - x\cos x)\right]^2$	$P(\theta) = \frac{1}{x}\int_0^{2x}\frac{\sin y}{y}dy - \left(\frac{\sin x}{x}\right)^2$	$P(\theta) = (2/x^2)(x - 1 + e^{-x})$

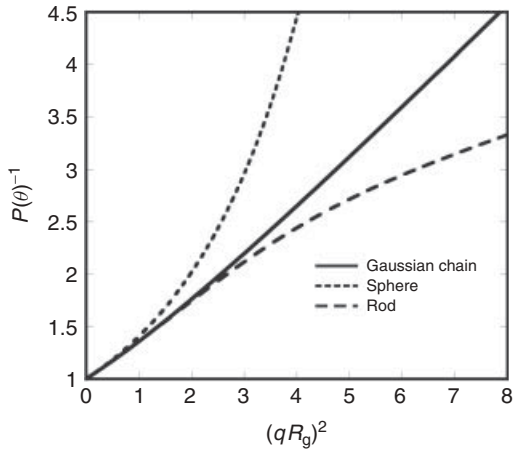

Figure 18.7 Calculated form factors for a Gaussian chain, sphere and a rod. The R_g's used were: for a homogenous sphere of radius a, $R_g^2 = 3/5\ a^2$ and for a rod of length L, $R_g^2 = L^2/12$.

Figure 18.7 shows the effects of structure on $P(\theta)^{-1}$. In the case of a rod, $P(\theta)^{-1}$ tends to grow slower with $q^2\left\langle R_g^2\right\rangle$. Therefore, for a wormlike chain, $P(\theta)^{-1}$ will lie between a flexible Gaussian chain and a rod. A similar effect occurs for a polydisperse sample of flexible chains because light scattering from the large molecules decays more rapidly with increasing angle than the scattering from small molecules, and therefore, their contribution becomes more significant at larger angles; hence, polydispersity and rigidity have qualitatively equivalent effects. The same applies to solvent effects; in good solvents, chains tend to swell and deviate from the Gaussian distribution and this concomitantly will make $P(\theta)^{-1}$ grow slower with $q^2\left\langle R_g^2\right\rangle$. The opposite happens for a homogenous sphere where $P(\theta)^{-1}$ tends to grow faster with $q^2\left\langle R_g^2\right\rangle$. Chain branching tends to give, for the same molecular weight, more compact structures, and therefore, $P(\theta)^{-1}$ will have a shape between a linear Gaussian chain and a sphere [41]. The influence of such factors on $P(\theta)^{-1}$ does not allow a unique interpretation of the structure of the macromolecule or the particle shape; one should have additional information from complementary independent characterization methods. It is interesting to note that independently of the shape, the initial slope is always 1/3.

In the opposite limit, for $q\xi \gg 1$, Benoit proved, for a Gaussian chain, that $P(\theta)^{-1}$ is still linear with q^2. In fact, in this limit, $P(\theta)^{-1} = 1/2\ \left(1 + q^2\left\langle R_g^2\right\rangle\right)$ [42]. For a polydisperse sample, in the limit $q\left\langle R_g^2\right\rangle^{1/2} \gg 1$, Equation 18.44 becomes

$$\left[\frac{Kc}{R_\theta^{ex}}\right]_{\substack{c=0 \\ q\left\langle R_g^2\right\rangle^{1/2}\gg 1}} = \frac{1}{2\langle M\rangle_n}\left(1 + Bq^2\right) \qquad (18.46)$$

where $B = \langle N\rangle_n\,\ell^2/6$, with ℓ and $\langle N\rangle_n$ being the monomer size and the number-average degree of polymerization, respectively, and $\langle M\rangle_n$ is the number-average molecular weight, defined as $\sum N_i M_i / \sum N_i$. This result was extended to rods by Holtzer, except that instead of q^2 dependence, he found a linear behavior with q [43]. In principle, this implies that for large q's one can obtain also the first moment of the distribution in molecular weight. However, in practice, for the wavelengths used in light scattering experiments, in the majority of the cases, this asymptotic limit will never be reached. Nevertheless, if instead, we do a scattering experiment with X-rays (with enough electron density contrast) or neutrons, using a deuterated polymer in solution, then we will certainly reach this asymptotic limit.

As an illustration of SLS, in what follows, we give some interesting examples of the application of this technique to study the structure of complex systems. Figure 18.8 shows the experimental results of Galinsky and Burchard [44] on the determination of $P(\theta)$ for a collection of seven samples of branched macromolecules in a solution of 0.5 N NaOH, prepared from potato starch by controlled acid degradation. Previously, Burchard [45] had derived a form factor for trifunctional polycondensation model without excluded volume effects, namely,

$$P(q) = \frac{1 + (C/3)\left(qR_g\right)^2}{\left[1 + ((1+C)/6)\left(qR_g\right)^2\right]^2} \qquad (18.47)$$

The parameter C increases with the molar mass and is related to the branching probability p. For self-similar structures, one expects that the particle topology does not vary with molar mass, that is, the form factor should be independent of molar mass. These nonrandomly branched

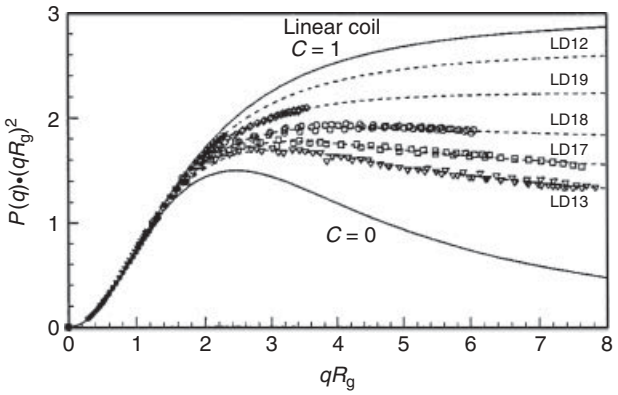

Figure 18.8 Kratky's plot of the form factor of samples of branched polymers derived from potato starch by controlled acid degradation. The upper continuous line corresponds to a linear chain ($C = 1$) while the lower one to a homogenously branched polymer ($C = 0$). *Source*: Reprinted with permission from Galinsky G, Burchard W. *Macromolecules* 1997;30:4445 [44]. Copyright 1997 American Chemical Society.

samples show only very limited intermediate range power law behavior. Furthermore, the various samples of different molar masses are not self-similar to each other, but each sample exhibits its own exponent in the asymptotic region. The Kratky representation of the data emphasizes the behavior at large qR_g and shows how well Equation 18.47 fits the experimental data with a single parameter.

Another interesting application, relevant to controlled drug release, is the determination of the outer diameter d and the membrane thickness δ as a function of pH of a sample of large polydisperse microcapsules ($\sim$10 μm) made of poly(L-lysine-*alt*-terephthalic acid). Dobashi et al. [46] showed that it is possible to measure $P(\theta)$ for individual particles with a new design of the sample cell (capillary tubing cell) and detecting system that could cover a range of q's from 0.5 to 6 μm^{-1}. By comparing the experimental $P(q)$ with the form factor for a spherical thin shell, they determined the values of d and δ as illustrated in Figure 18.9. The authors found that the lowest values for d and δ corresponded to pH 4 and increase as the pH differs from 4. They also established that d and δ change approximately proportional to each other suggesting an isotropic volumetric phase transition.

In the previous example, the microspheres were far greater than q^{-1}, and therefore, Dobashi et al. were able to resolve fine details. However, this is not always the case and we have to use complementary techniques such as SAXS or SANS to cover a wider range of q's.[3] An example of this is the study by Lonetti et al. [47] of wormlike micelles of a block copolymer of poly(butadiene-*co*-ethylene oxide) (PB-PEO) in water; these structures have a very broad range of length scales ranging from the contour and persistence length to the core/corona diameter and aggregation number per unit length (number of copolymer molecules per PB-core length of the worm). For the weight fraction of PEO w_{PEO} between 0.47 and 0.59, this system self-assembles in water as wormlike micelles with a core of PB and a corona of PEO, while for $w_{PEO} > 0.6$ and $w_{PEO} < 0.47$, they form spherical micelles and bilayers, respectively. However, a different way of tuning these morphological transitions is through solvent selectivity using a mixture of solvents. Lonetti et al. used in their work a mixture of N, N-dimethylformamide (DMF) and water and studied the relation between the smallest relevant length scale, as the diameter and aggregation number per unit length, to changes in the mesoscopic structure, that is, the contour and persistent lengths of the wormlike micelles; they also analyzed the transition from wormlike to spherical micelles. Figure 18.10 shows the experimental scattering intensities as a function of q for different solvent compositions of d-DMF and D_2O. The filled symbols correspond to SLS data, while the open symbols refer to SANS. For high water content, at low q values, the scattering intensity scales as q^{-1} (SLS region), corresponding to rigid rods, independent of the micelle length, polydispersity, and flexibility. No sign of q^{-2} dependence typical of wormlike micelles is observed in view that the persistence length is larger than 500 nm. At d-DMF mole fraction, $f_{d\text{-}DMF} > 0.09$, the low q data shows a change in q dependence allowing to obtain information about the persistence length. We also observe that as the DMF content increases, the minima of the oscillation in the form factor move toward larger q's indicating a smaller overall cylinder diameter. From Figure 18.10, they could infer qualitatively a transition to spherical micelles. By adding DMF until $f_{d\text{-}DMF} = 0.5$, a 50% decrease in the scattering intensity is reported, with no change in slope. From $f_{d\text{-}DMF} = 0.7$, the intensity becomes independent of q forming a plateau, representative of the scattering by spherical objects. Using the Kholodenko model to fit the data and other complementary techniques, Lonetti et al. were able to obtain information about the core/corona diameter, the aggregation number per unit length, the density gradient of the shell, the contour, and the persistence length [48].

These examples show the potential that scattering techniques have in determining thermodynamic and structural features of rather complex polymeric systems. However, they also show that if we want to go beyond the determination of molecular weight and average radius of gyration, theoretical modeling is necessary to interpret the scattering data and obtain more information about the system. More examples of the application of SLS and DLS, including a

[3]The theoretical framework of both techniques is the same as the one discussed for light scattering except for the front factor. For SAXS or SANS, the intensity will be related to the correlation of electron densities or nuclei densities, respectively.

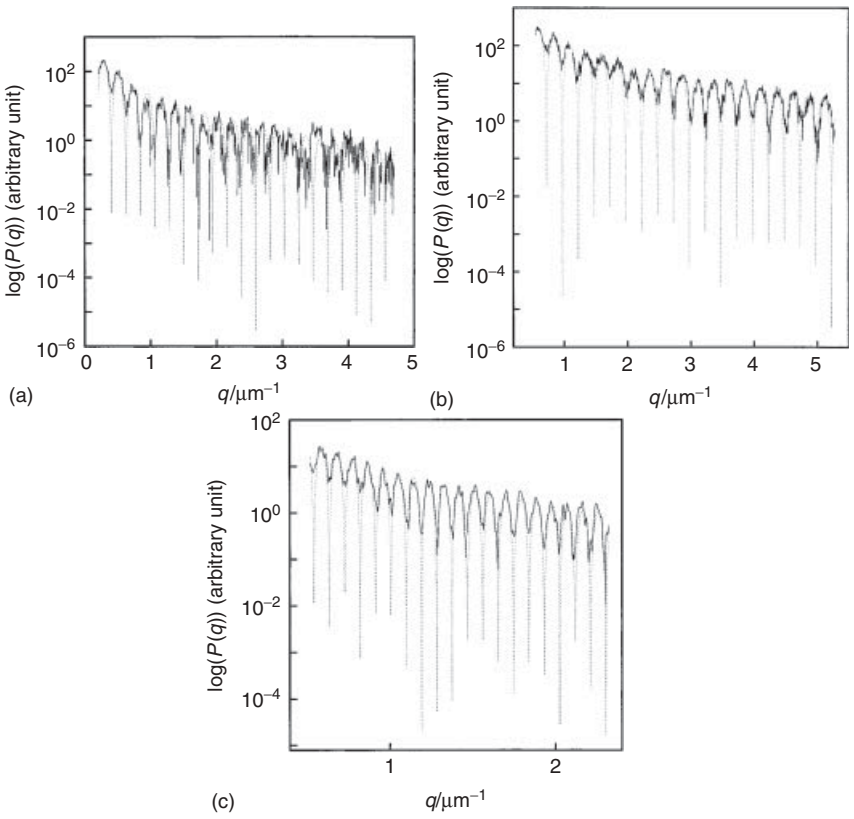

Figure 18.9 Observed (solid curve) and calculated (dotted curve) scattering pattern of microcapsules with (a) pH = 2, (b) pH = 4, and (c) pH = 10. *Source*: Reprinted with permission from Dobashi T, Narita T, Masuda J, Makino K, Mogi T, Ohshima H, Takenaka M, Chu B. *Langmuir* 1998;14:745 [46]. Copyright 1998 American Chemical Society.

discussion of experimental details, can be found in Schärtl's book [49].

18.4 DYNAMIC LIGHT SCATTERING

18.4.1 General Concepts: Determination of Particle Sizes in Dilute Solutions

In order to observe the time dependence of the scattered intensity, certain experimental conditions must be met. First, the characteristic time of a fluctuation is rather short and therefore requires special detectors that can respond to such timescale. Second, the scattering volume should be small and the angle subtended on the detector should also be small so that the area seen by the detector is on the order of one coherence area (which is the zone where the light is almost in phase producing constructive interference). Rephrasing the previous statements, if we illuminate with a laser a cell filled with a sample of a suspension of scattering particles, we will observe a "speckle pattern"(bright spots) that is constantly changing due to the motion of the particles; experimentally, we should observe a volume on the order of a single "speckle." The timescale of the fluctuations depends on the time that takes a particle to move a distance of the probing effective wavelength ($\lambda/\sin(\theta/2)$). This time depends on the size and geometry of the scattering objects, the fluid viscosity, the temperature, and the concentration.

There are basically two approaches for the measurement of the time dependence of the scattered intensity. The first one is addressed to processes that are rather fast, which require the Fabry–Perot interferometers or diffraction gratings to obtain the spectral decomposition of the scattered light. These devices are placed in between the scattering cell and the detecting system and act as a filter. By varying the spacing or other setting parameter, we can make a spectral decomposition of the scattering intensity and obtain $I(\mathbf{q}, \Delta\omega)$, as in Equation 18.5. However, these techniques do not have the resolution to study processes slower than 10^{-6} s. Diffraction gratings resolve adequately when the dynamics is faster than 10^{-10} s, while Fabry–Perot interferometer is the right choice for the process in between 10^{-6} and 10^{-10} s. On the other hand, in common applications, the timescale ranges from

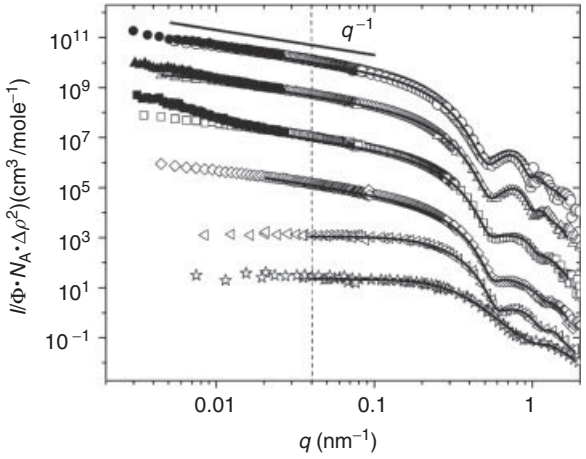

Figure 18.10 Experimental and fitted lines as a function of q of the scattered intensity by PB-PEO block copolymer in different solvent whose compositions go from d-DMF to D_2O. (open symbols SANS, filled symbols SLS). Circle, pure D_2O; up triangle, $f_{\text{d-DMF}} = 0.09$; square, $f_{\text{d-DMF}} = 0.36$; diamond, $f_{\text{d-DMF}} = 0.5$; left triangle, $f_{\text{d-DMF}} = 0.7$; star, pure d-DMF. The dashed line indicates the range of fit of SANS data. For the sake of clarity, data were shifted by arbitrary factors. *Source*: Reprinted with permission of Lonetti B, Tsigkri A, Lang PR, Stellbrink J, Willner L, Kohlbrecher J, Lettinga MP. Macromolecules 2011;44:3583 [47]. Copyright 2011 American Chemical Society.

10^{-7} to 1 s. If this is the case, we use the so-called optical mixing techniques (OMTs), also called *photon correlation spectroscopy* (*PCS*). In PCS, the scattered light is directly collected by the detector; if the previously discussed experimental conditions are met, then we will have a highly fluctuating scattered intensity with time as the output. In the homodyne (or self-beat) method, only the scattered light is collected, while in the heterodyne method, we mix in the detector the scattering light with another nonscattered light, normally a small portion of the incident beam. Furthermore, the statistical analysis of the fluctuating scattered intensity is done by means of a digital correlator. For the homodyne arrangement, the final output will be then the correlation function between intensities

$$G_2(\mathbf{q}, \tau) = \lim_{T\to\infty} \frac{1}{T} \int_0^T I_s(\mathbf{q}, t) I_s(\mathbf{q}, t+\tau) \mathrm{d}t \qquad (18.48)$$

If the process is stationary and ergodic, the time average can be replaced by an ensemble average, $G_2(\mathbf{q}, \tau) = \langle I_s(\mathbf{q}, \tau) I_s(\mathbf{q}, 0)\rangle$. Experimentally, $G_2(\mathbf{q}, t)$ is determined by recording $I_s(t)$ at time intervals much shorter than the timescale of typical fluctuations and accumulating the products of the intensities as a function of the sampling time τ. The sampling can be chosen to be linear or exponential. Actually, the exponential sampling is the best choice.

If we assume the scattered electric field as a superposition of a large number of statistically independent random electric fields, then according to the central limit theorem, the scattered field will be a random field with a Gaussian distribution. This is called the *Gaussian approximation*, which is valid in many cases. However, this will not be satisfied, for example, in strongly interacting particles, or in nonergodic systems such as gels. Within the Gaussian approximation, $G_2(\mathbf{q}, t)$ can be written in terms of the autocorrelation function between the scattered fields $G_1(\mathbf{q}, t) = \langle E_s(\mathbf{q}, \tau) E_s(\mathbf{q}, 0)\rangle$ as

$$G_2(\mathbf{q}, t) = B + f \left| G_1(\mathbf{q}, \tau) \right|^2 \qquad (18.49)$$

which is known as the *Siegert relationship*. Here, B is the baseline $\langle I_s(\mathbf{q}) I_s(\mathbf{q})\rangle$ and f is the spatial coherent factor that depends on the number of coherent areas in the detector and will be equal to 1 for a single coherent area or less [50–52].

Although homodyne is the most used method in PCS, we describe shortly also the heterodyne method, which is widely used for Doppler velocimetry experiments or when the Siegert relation is not applicable. Heterodyning means that we mix in the detector the scattered light with a strong nonscattered signal (named commonly as the *local oscillator*), that is,

$$\langle I_s(\mathbf{q}, t) I_s(0)\rangle = \left\langle \left| E_{LO} + E_s(\mathbf{q}, t) \right|^2 \left| E_{LO} + E_s(\mathbf{q}, 0) \right|^2 \right\rangle \qquad (18.50)$$

Since $E_{LO} \gg E_s$, we can approximate $\langle I_s\ (t)\ I_s\ (0)\rangle$ as

$$\langle I_s(\mathbf{q}, t) I_s(0)\rangle \cong \left[I_{LO}^2 + 2 I_{LO}\ \mathrm{Re} G_1\ (\mathbf{q}, t) \right] \qquad (18.51)$$

This means that in most applications, we can relate $G_2(\mathbf{q}, t)$ to $G_1(\mathbf{q}, \tau) = \langle E_s(\mathbf{q}, \tau) E_s(\mathbf{q}, 0)\rangle$ by either homodyne or heterodyne methods. Proceeding in the same way as in the SLS, we can relate $\langle \Delta\varepsilon(\mathbf{R}, t) \Delta\varepsilon(\mathbf{0}, \mathbf{0})\rangle$ with the dynamic joint probabilities $G_{\text{intra}}(\mathbf{R}, t)$ and $G_{\text{inter}}(\mathbf{R}, t)$ and write Equation 18.5 as

$$I_s(\mathbf{q}, \Delta\omega) \cong \left\{ \frac{1}{n} \int G_{\text{intra}}\ (\mathbf{R}, t)\ \mathrm{e}^{(-i(\mathbf{q}\bullet\mathbf{R} + \Delta\omega t)} \mathrm{d}\mathbf{R}\mathrm{d}t \right\} + N_A c \left\{ \int \left(g_{\text{inter}}\ (\mathbf{R}, t) - 1 \right) \mathrm{e}^{(-i(\mathbf{q}\bullet\mathbf{R} + \Delta\omega t)} \mathrm{d}\mathbf{R} \right\} \qquad (18.52)$$

Equation 18.52 becomes the dynamic equivalent of Equation 18.35 where $G_{\text{intra}}(\mathbf{R}, t)$ is the probability of finding any monomer at $\mathbf{R}$ at time t when any other of the *same* macromolecule is at the origin at $t = 0$, while $G_{\text{inter}}(\mathbf{R}, t)$ is the joint probability of finding any monomer at $\mathbf{R}$ at time t when any monomer of a *different* macromolecule is at the origin at $t = 0$. In Equation 18.52,

$g_{\text{inter}}(\mathbf{R}, t) = G_{\text{inter}}(\mathbf{R}, t)/\langle\rho_1\rangle$. For a dilute solution, this reduces to

$$I_s(\mathbf{q}, \Delta\omega) \cong \int G_{\text{intra}}(\mathbf{R}, t)\, e^{(-i(\mathbf{q}\bullet\mathbf{R}+\Delta\omega t)} d\mathbf{R}dt \quad (18.53)$$

We have omitted all the front factors since they are not relevant for the time dependence of the scattering intensity.

Let us now consider the simplest case, a system consisting of diluted suspension of spheres, such as a latex particle suspension. As with any rigid body, there will be only two dynamic modes: a translation of the center of mass and the rotation around the center of mass. For a sphere, the only mode that participates in the fluctuations in concentration will be the translational one since a rotation around the center of mass will have no effect on mass transfer in a scattering volume element. This means that in the case of a sphere, we can factorize $G_{\text{intra}}(\mathbf{R}, t)$ as

$$G_{\text{intra}}(\mathbf{R}, t) = G_{\text{intra}}(\mathbf{R}')P(\mathbf{r}_{\text{cm}}, t) \quad (18.54)$$

where $\mathbf{r}_{\text{cm}}$ is the position vector of the center of mass and $\mathbf{R}'$ is the position vector of any point in the sphere relative to the center of mass $\left(\mathbf{R} = \mathbf{R}' + \mathbf{r}_{\text{cm}}\right)$. Substituting Equation 18.54 into Equation 18.53, we can factorize $I_s(\mathbf{q}, \Delta\omega)$ as

$$I_s(\mathbf{q}, \Delta\omega) \approx P(\theta)\left[\int P(\mathbf{r}_{\text{cm}}, t) e^{-i(\mathbf{q}\bullet\mathbf{r}_{\text{cm}}+\Delta\omega t)} d\mathbf{r}_{\text{cm}}dt\right] \quad (18.55)$$

$P(\theta)$ is the form factor for a sphere already discussed and $P(\mathbf{r}_{\text{cm}}, t)$ is the probability that the center of mass of a sphere is at $\mathbf{r}_{\text{cm}}$ at time t when at $t = 0$ was at the origin.

To illustrate, let us assume that the particles all move at constant velocity $\mathbf{v}_0$. Then $P\left(\mathbf{r}_{\text{cm}}, t\right)$ is given by

$$P\left(\mathbf{r}_{\text{cm}}, t\right) \approx \delta\left(\mathbf{r}_{\text{cm}} - \mathbf{v}_0 t\right) \quad (18.56)$$

and spectral decomposition of the scattered intensity is

$$\begin{aligned} I_s(\mathbf{q}, \Delta\omega) &\approx P(\theta)\left[\int e^{i(\pm\mathbf{q}\bullet\mathbf{v}_0-\Delta\omega)t} dt\right] \\ &\approx P(\theta)\left[\delta\left(\Delta\omega + \mathbf{q}\bullet\mathbf{v}_0\right) + \delta\left(\Delta\omega - \mathbf{q}\bullet\mathbf{v}_0\right)\right] \end{aligned} \quad (18.57)$$

that is, in frequency space, we will observe two sharp spikes at $\omega_0 \pm \mathbf{q} \cdot \mathbf{v}_0$, as shown in Figure 18.11. This means that if we illuminate with a frequency ω_0, the scattered light will suffer a Doppler shift from the incident frequency by $\pm\mathbf{q} \cdot \mathbf{v}_0$. Since we know $\mathbf{q}$, we can determine $\mathbf{v}_0$ by DLS.

Now, let us consider the case of spherical particles diffusing in a medium; the equation governing $P\left(\mathbf{r}_{\text{cm}}, t\right)$ will be Fick's law

$$\frac{\partial P\left(\mathbf{r}_{\text{cm}}, t\right)}{\partial t} = D\nabla^2 P\left(r_{\text{cm}}, t\right) \quad (18.58)$$

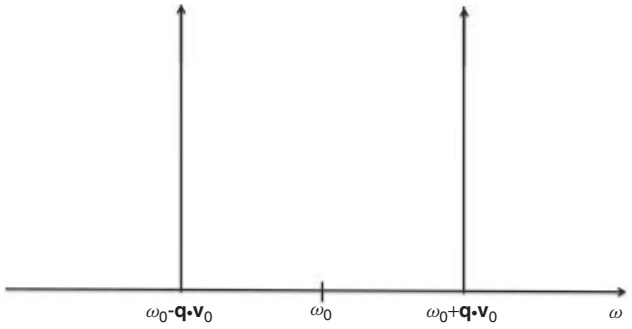

Figure 18.11 Spectral decomposition of the scattered light by spheres moving at constant velocity.

where D is the diffusion coefficient. The solution in q space is

$$P(\mathbf{q}, t) \approx e^{-q^2 Dt} \quad (18.59)$$

Therefore, the time dependence of the scattered intensity is

$$I_s(\mathbf{q}, t) \approx e^{-q^2 Dt} \quad (18.60)$$

This is probably the most emblematic expression in DLS (Fig. 18.12).

As we can see, the decay time $\tau = 1/(q^2 D)$ is nothing else than the time that it takes for a Brownian particle to cross a distance $\sqrt{6/q}$.

Equation 18.60 is valid for any object that follows a *translational* diffusion no matter what its actual form is. If the object is not a rigid sphere then will have other dynamical modes that contribute to the fluctuations in the scattered field, such as rotational diffusion, elastic modes, which will also contribute to the scattered intensity, as discussed later.

The decay constant can be written in terms of the particle size using the Stokes–Einstein relationship

$$D = \frac{k_B T}{\zeta} \quad (18.61)$$

where ζ is the friction coefficient. In the case of a sphere $\zeta = 6\pi\eta R$, where R is the radius of the sphere and η is the viscosity of the medium. When the diffusing particles are not hard spheres, it is common to introduce the concept of the hydrodynamic radius R_h that is the radius of an equivalent hard sphere with the same translational diffusion as the scattering object, whether this is a macromolecule, a rod, or any other form.

Thus, the decay time of the normalized correlation function $g_1(\mathbf{q}, t) = \langle E(\mathbf{q}, t)E(\mathbf{q}, 0)\rangle / I_s(\mathbf{q})$ for a monodisperse sample of spheres is

$$\tau = \frac{1}{q^2 D} = \frac{6\pi\eta R}{q^2 k_B T} \quad (18.62)$$

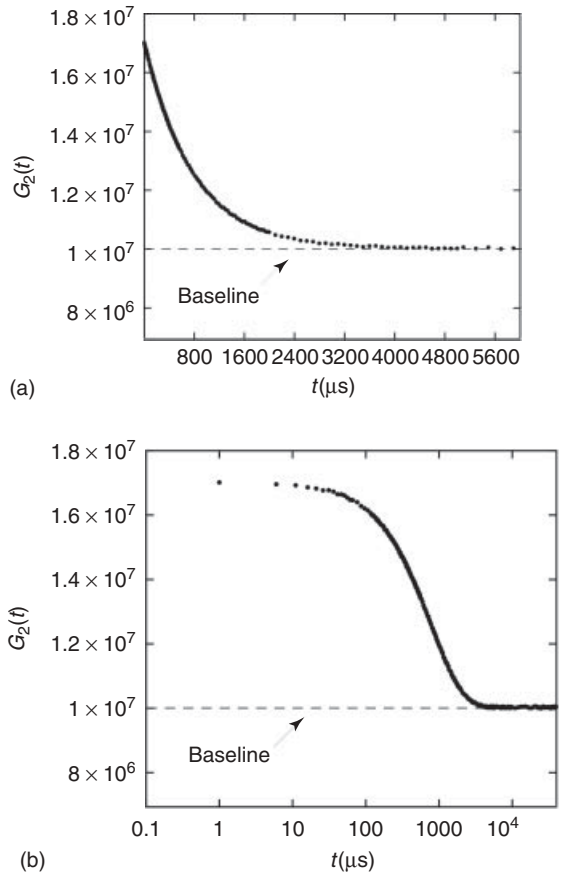

Figure 18.12 Typical $G_2(t)$ display for a monodisperse latex sample of 400 nm particle diameter. (a) Linear plot and (b) logarithmic plot.

Since q, T, and η are known, we determine R from the measurement of τ. Actually, most commercial software calculate the size assuming that the object is spherical. As mentioned before, the digital correlator gives directly $G_2(\mathbf{q}, t)$, and therefore, after subtracting the baseline and dividing by baseline, we get by the Siegert relationship a correlation function $C(t)$ given by

$$C(t) = \frac{G_2(t) - B}{B} = f\mathrm{e}^{-2q^2Dt} \tag{18.63}$$

Notice that in a homodyne experiment the decay time is *twice* of that in a heterodyne experiment. This means that when we perform a homodyne experiment, we must be sure that no stray light reaches the detector, otherwise we might have a mixture of homodyne–heterodyne output. A thorough discussion of the instrumental considerations to be followed when using DSL is found in Reference 52.

In the case of a polydisperse sample of spheres, each particle size contributes to the scattered intensity following the time dependence shown in Equation 18.60, giving rise to a superposition of exponential decays; the specific contribution of each species to the total light scattered is proportional to the scattered intensity by the particles of the species, that is,

$$I_s(\mathbf{q}, t) \approx \sum_i I_{si}(\mathbf{q})\mathrm{e}^{-q^2D_it} \tag{18.64}$$

Writing Equation 18.64 in terms of $g_1(\mathbf{q}, t)$ we have

$$g_1(\mathbf{q}, t) = \frac{\sum_i I_{si}(\mathbf{q})\mathrm{e}^{-q^2D_it}}{\sum_i I_{si}(\mathbf{q})} \tag{18.65}$$

To simplify the notation, we omit in the following discussion the explicit $\mathbf{q}$ dependence in I_s and g_1 and use a single parameter $\Gamma = q^2D$ to identify the species; in that case, we can rewrite Equation 18.65 as:

$$g_1(t) = \int_0^\infty G(\Gamma)\mathrm{e}^{-\Gamma t}\mathrm{d}\Gamma \tag{18.66}$$

which is the Laplace transform of $G(\Gamma)$ that is given by

$$G(\Gamma) = \frac{\sum_i I_{si}\delta\left(\Gamma - \Gamma_i\right)}{\sum_i I_{si}} \tag{18.67}$$

All the information on the distribution is in G, while $g_1(t)$ is experimentally determined using the Siegert relation. To extract from $g_1(t)$ the size distribution, one has to invert Equation 18.66; however, this type of linear transformations are known to be ill-conditioned, that is, if the experimentally measured $g_1(t)$ contains any noise, the solution for $G(\Gamma)$ is not unique. We can only expect to have a poor-resolution picture of $G(\Gamma)$ and we will never retrieve the fine details of the distribution. The mathematical reasons for this were studied by McWhirter and Pike [53] who solved the eigenvalue problem of the Fredholm equation of the first class with the Laplace kernel. They prove that the eigenfunctions are mutually orthogonal and form a complete set; they also obtained the eigenvalue spectrum for the Laplace transform $\lambda_\mu^\pm$ and found that they decay exponentially with μ. The latter is the fundamental reason why it is impossible to recover a high resolution $G(\Gamma)$; any small noise in $g_1(t)$ will give rise to a large noise in $G(\Gamma)$. In such circumstances, it is not possible to obtain a complete and unique result.

In spite of the ill-conditioned inversion problem, there are a good number of approaches that try to overcome the inherent limitations by proposing schemes that can provide some information about the distribution function. The simplest and oldest of all DSL data analysis methods is

the method of cumulants [54]. The essence of this method lies in expanding $\exp(-\Gamma t)$ in Equation 18.66 about the mean value $\langle\Gamma\rangle$, where $\langle\Gamma\rangle$ is defined as

$$\langle\Gamma\rangle = \int_0^\infty \Gamma G(\Gamma)\mathrm{d}\Gamma \tag{18.68}$$

Then,

$$g_1(t) = \exp\left(-\langle\Gamma\rangle t\right)\left[1 + \frac{\mu_2 t^2}{2!} - \frac{\mu_3 t^3}{3!} + \cdots\right] \tag{18.69}$$

where

$$\mu_i = \int_0^\infty (\Gamma - \langle\Gamma\rangle)^i\, G(\Gamma)\mathrm{d}\Gamma \tag{18.70}$$

are the ith moments about the mean (cumulants) of $G(\Gamma)$. $\langle\Gamma\rangle$ can be obtained directly from $g_1(t)$ as

$$\langle\Gamma\rangle = -\left[\frac{\mathrm{d}g_1(t)}{\mathrm{d}t}\right]_{t=0} \tag{18.71}$$

Since the weighting factors in $G(\Gamma)$ are the I_{si}'s, we know from the SLS discussion that $I_{si}(\mathbf{q}) \approx N_i M_i^2 P_i(q)$, where N_i and M_i are the number and mass of species i, respectively, while $P_i(q)$ is its form factor. Substituting the expression for I_{si} in Equation 18.68 leads to

$$\frac{\langle\Gamma\rangle}{q^2} = \frac{\sum_i N_i M_i^2 P_i(q) D_i}{\sum_i N_i M_i^2 P_i(q)} \tag{18.72}$$

This is sometimes called the *apparent diffusion coefficients* $D_{\mathrm{app}}(q)$ since it depends on q. If the particle sizes are small compared to λ, or if we observe at very small angles, then $P(q) \to 1$ and Equation 18.72 reduces to

$$\frac{\langle\Gamma\rangle}{q^2} = \frac{\sum_i N_i M_i^2 D_i}{\sum_i N_i M_i^2} = \langle D\rangle_z \tag{18.73}$$

Normally, $\langle D\rangle_z$ is obtained by taking several measurements of $D_{\mathrm{app}}(q)$ at different angles and extrapolating to zero angle. In terms of the hydrodynamic radius, Equation 18.73 implies that in the limit of $q \to 0$, $\langle\Gamma\rangle/q^2 = \left(k_{\mathrm{B}}T/6\pi\eta\right)\left\langle R_{\mathrm{h}}^{-1}\right\rangle_z$.

From Equation 18.70, μ_2 can be written as the variance of Γ : $\mu_2 = \langle\Gamma^2\rangle - \langle\Gamma\rangle^2$. In the limit of small angles, we can write the so-called polydispersity index (PI), $\mu_2/\langle\Gamma\rangle^2$ as

$$\frac{\mu_2}{\langle\Gamma\rangle^2} = \frac{\left\langle D^2\right\rangle_z - \langle D\rangle_z^2}{\langle D\rangle_z^2} \tag{18.74}$$

In view of McWhirter and Pike's work, noise will limit the number of cumulants that we can actually measure. In most cases, only $\langle\Gamma\rangle$ and μ_2 can be determined. Cumulants are used for monomodal size distributions that have a PI not larger than 0.3. In bimodals or other more complex distributions, cumulant analysis will be meaningless and will only give some type of rough screening of the data. Even more, $D_{\mathrm{app}}(q)$, which is what is usually determined, is also dependent on the type of correlator, whether linear or nonlinear correlator, and the number of channels used [55].

Ostrowsky et al. [56] proposed one of the first methods of inverting Equation 18.66. On the basis of the previous work of McWhirter and Pike, mentioned before, they suggested replacing Equation 18.66 by a sum of exponentials whose Γ's are spaced exponentially according to

$$\Gamma_{n+1} = \Gamma_n \exp\left(\frac{\pi}{\omega_{\max}}\right) \tag{18.75}$$

where $\omega_{\max}$ is a parameter determined by the noise level of the correlation function. The number of exponentials used in the reconstruction depends also on the noise level.

The amplitudes of the histogram of the distribution function are calculated by a non-negative least square method. This procedure is known as the *exponential sampling method* and is applicable to both monomodal and bimodal distributions. However, in view of the limitations of the Laplace inversion, it is difficult to resolve bimodal distributions with a ratio between the two particle species below 2.

Provencher has developed an effective inversion software package, CONTIN, which is a generalized inverse Laplace transform with constraints. CONTIN also turns $g_1(t)$ into a discrete sum of exponentially spaced set of exponential; however, it includes additional constrains in order to suppress artificial oscillations. For that purpose, it uses a constraint regularization term, which limits solutions with high curvatures (constraints on the second derivatives) [57, 58]. This software is included in all commercial instruments. Other approaches that have been used are maximum entropy, Regularized Positive Exponential Sum (REPES), single value decomposition, multiangle constrained inversion, Bayesian inversion method together with multiangle DSL (MDSL), to mention some [59–65].

A general comment that applies to all the inversion methods is that when they are used as a black box (as they are normally used), one should take the result only as indicative of the distribution. The ill-conditioned nature of the inversion problem together with uncontrolled factors and artifacts of the inversion method used can lead to false particle size distributions. In any case, in spite of the inherent limitations of any of these methods, a well-trained researcher in DLS can profit from these methods as optimized inversion tools.

18.4.2 Dynamic Light Scattering by a Dilute Solution of Thin Rods

Let us consider now a system consisting of thin rods suspended in a fluid at a concentration regime where the rods do not interact between each other. This particular geometry is important since there are many biological molecules, which, as a first approximation, can be described as rigid rods, such as helical polypeptides, some proteins, and tobacco mosaic virus (TMV). Also, important new nanotechnological products such as organic or inorganic nanotubes or nanorods with a large aspect ratio are good examples of rodlike particles. For this geometry, two types of motions contribute to the fluctuations in the scattered intensity. The first one is again related to the translational motion of the rod, while the second dynamic mode is associated with the rotation of the rod around the center of mass of the rod.

The first to calculate the time dependence of the scattering intensity of thin rods was Pecora [66, 67]. He introduced some simplifications assuming that the translational and the rotational dynamics were not coupled and that the thickness of the rod is negligible compared with the wavelength. The mathematical details of his derivation can be found in Berne and Pecora's book [50]. His final result for the scattered intensity time dependence for a VV configuration is[4]

$$I_s^{VV}(\mathbf{q}, t) \approx S_0(qL)\exp\left[-q^2Dt\right] + S_1(qL)\exp\left[-\left(q^2Dt + 6D_r t\right)\right] + \cdots \tag{18.76}$$

where L is the length of the rod, D is the translational diffusion coefficient of the center of mass, and D_r is the rotational diffusion coefficient. $S_0(qL)$, $S_1(qL)$, ... are the sums of the Bessel functions. What is interesting from his result is that for $qL \leq 3$, $S_0(qL)$ is much greater than any other terms and therefore we can neglect them. This implies that at very small angles or L small compared with λ, the time dependence of the scattered intensity will be fully dominated by the translational diffusion. On the other hand, for $qL \geq 5$, $S_1(qL)$ becomes relevant; its contribution to $I_s^{VV}(\mathbf{q}, t)$ for $qL = 5.2$ is 12% and is 57% for $qL = 10$. The rest of the terms in the series are negligible up to $qL \leq 8$. This means that we can determine the translational diffusion, extrapolating $D_{app}(q)$ to zero angle. At higher angles, the second term becomes relevant and using the value of D previously determined we can measure the rotational diffusion coefficient D_r.

[4]VV stands for an incident beam vertically polarized, and we observe the vertically polarized component of the scattered field. In the VH configuration, we observe the cross-polarized component of the scattering field for a vertical polarization of the incident beam.

In general, the diffusion equation for a rod with finite thickness contains the coupling of translational and rotational motions. A lucid account of this topic can be found in Doi and Edwards' book [68]. Wilcoxon and Schurr [69] and, independently, Maeda and Fujime [70] have studied the theory of DLS by thin rodlike particles. Although the explicit autocorrelation function can only be obtained numerically, the first cumulant can be derived readily

$$\frac{\langle\Gamma\rangle}{q^2} = D - \Delta\left[\frac{1}{3} - f_2\left(\frac{qL}{2}\right)\right] + \frac{L^2}{12}D_r f_1\left(\frac{qL}{2}\right) \tag{18.77}$$

where $D = (1/3)(D_\parallel + 2D_\perp)$ is the translational diffusion coefficient of the center of mass; $D_\parallel$ and $D_\perp$ are the translational diffusion coefficients parallel and perpendicular to the axis of the rod, respectively; and $\Delta = D_\parallel - D_\perp$. The functions $f_1(qL/2)$ and $f_2(qL/2)$ are given numerically by Maeda and Fujime and analytically by Hammouda [71]. When $qL \ll 1$, $f_1(qL/2)$ and $f_2(qL/2)$ tend to be 0 and 1/3, respectively, and we recover Pecora's result for small qL values where translational diffusion of the center of mass is the dominant dynamical mode. In contrast, for $qL \gg 1$, $f_1(qL/2)$ and $f_2(qL/2)$ approach 1 and 0, respectively, and $\langle\Gamma\rangle/q^2 \to D_\perp + (L^2/12)D_r$.

$D_\parallel$ and $D_\perp$ and D_r are related to the length L and the diameter d of the rod as

$$D_\parallel = \left(\frac{k_B T}{2\pi\eta L}\right)\left[\ln(p) + \nu_\parallel(p)\right] \tag{18.78}$$

$$D_\perp = \left(\frac{k_B T}{4\pi\eta L}\right)\left[\ln(p) + \nu_\perp(p)\right] \tag{18.79}$$

$$D_r = \left(\frac{3k_B T}{\pi\eta L^3}\right)\left[\ln(p) + \nu_r(p)\right] \tag{18.80}$$

where p is the aspect ratio of the rod $p = L/d$, η is the viscosity of the solvent, and the functions ν's are end-effect corrections and have been calculated by several authors [72]. This implies that for thin rods that have a length comparable to the wavelength, it is possible to determine by DSL all diffusion coefficients and their geometrical dimensions.

Throughout this discussion, we have implicitly assumed that the rod is optically homogenous with a single index of refraction and that the Rayleigh-Debye-Gans theory is valid, which basically restricts the theory to thin rods, unless the refractive index of the cylinder is close to that of the solvent used [73].

In a depolarized dynamic light scattering (DDLS) experiment in the VH configuration, we observe the cross-polarized component of the scattering field produced by a vertically polarized incident beam with respect to the scattering plane. In this case, the purely translational

particle motion does not contribute to I_{sVH} and for small qL values, the only term that survives will be

$$I_{sVH}(\mathbf{q}, t) \approx S_{VH}(qL) \exp\left[-\left(q^2 D + 6D_r\right) t\right] \quad (18.81)$$

Therefore, by plotting $\langle\Gamma\rangle$ against q^2 and extrapolating to $q = 0$, we can determine D_r, whereas the slope of the linear regression of the fitted data gives us the value of D.

A drawback of DDLS experiments is the low intensity of the depolarized signal that requires the use of high power lasers; however, heating of the sample will be the limiting factor on how intense the primary beam can be. Therefore, special care must be taken to avoid all types of possible extra signals that could enter the detecting system. DDLS experiments can have very short decay times, depending on the timescale of the motion of the particles in solution. For timescales of 50 ns and faster, which is usually valid for molecules with a molecular weight of less than 50,000 Da, interferometric methods are recommended. For larger particles, the usual homodyne photon correlation techniques can be applied.

Lehner et al. [74] have compared DLS and DDLS methods in the determination of D, D_r, and Δ for TMV, a well-characterized biological model for these types of techniques. TMV is a rigid cylinder of 300 nm length and 18 nm diameter with a molecular weight of 4×10^{-7} Da and it is highly uniform in size with a normalized variance (PI) much less than 0.1. In a dilute concentration sample (0.245 g/l of TMV in pure water), it is necessary to add a small concentration of salt (2×10^{-3}M NaCl solution) to screen out the surface charges of TMV. Figure 18.13 shows a comparison of the DDLS results with and without the addition of salt. While the D_r value remains almost unchanged after addition of salt, a significant increase in the slope, and hence in D, is observed. With the added salt solution, the authors obtained values of 299 ± 9 s^{-1} and $(4.05 \pm 0.09) \times 10^{-12}$ m^2/s for D_r and D, respectively.

Furthermore, they compared the DDLS results with a DLS measurement fitting the experimental data with Equation 18.77. Figure 18.14 shows a plot of $\langle\Gamma\rangle/q^2 (=D_{eff})$ against q^2; the solid line corresponds to a fit where they fixed D_r to the value obtained by DDLS and left D and Δ as free-fitting parameters. Following this procedure, they found D to be around 5% higher than the value obtained by DDLS and Δ was close to the value reported by Wilcoxon and Schurr by DLS [69]. They also followed a different procedure where D and D_r were taken from the DDLS measurements and only left Δ as a free-fitting parameter (dashed line); however, in this case, the Δ obtained was 40% lower than that obtained by the first method. Hydrodynamic theories lead to a Δ of approximately 1.8×10^{-12} m^2/s, which is close to the value obtained by the first method (1.79×10^{-12} m^2/s) [72]. They attributed this difference to the lowest angle considered in the second procedure (20°) and suspected that some stray light coming from dust could contaminate the detected signal.

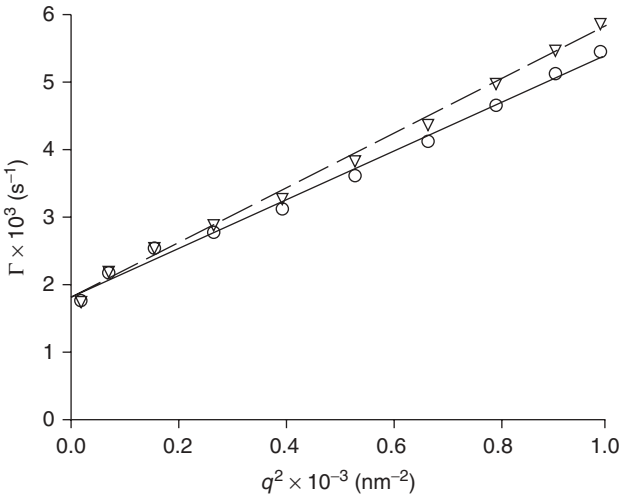

Figure 18.13 Comparison of the decay rate Γ with q^2 from DDLS data of a 0.245 g/l TMV solution in pure water (◯) and in 2×10^{-3} M NaCl solution (▽) at 20 °C. *Source*: Reprinted with permission from Lehner D, Lindner H, Glatter O. *Langmuir* 2000;16:1689 [74]. Copyright 2000 American Chemical Society.

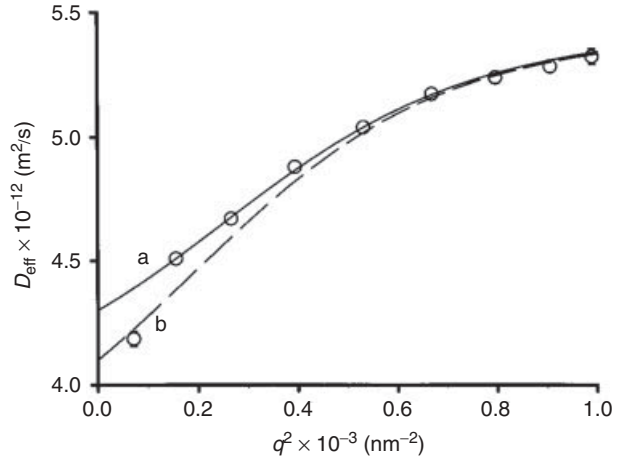

Figure 18.14 DLS data ($D_{eff} = \langle\Gamma\rangle/q^2$ vs q^2) of a 2×10^{-3} M NaCl solution of TMV at a concentration of 0.245 g/l at 20 °C (◯). (a) $D = 4.3 \times 10^{-12}$ m^2/s, $D_r = 300$ s^{-1}, and $\Delta = 0.41\ D$ (full line); (b) $D = 4.1 \times 10^{-12}$ m^2/s, $D_r = 300$ s^{-1}, and $\Delta = 0.25\ D$ (dashed line). *Source*: Reprinted with permission from Lehner D, Lindner H, Glatter O. *Langmuir* 2000;16:1689 [74]. Copyright 2000 American Chemical Society.

18.4.3 Dynamic Light Scattering by Flexible Polymers

Following the line of discussion, the next step is to consider a system with more degrees of freedom, such as a deformable body, which besides the translational and

rotational "modes," can also have elastic modes. This can be a gel, a polymer melt, or a single polymer chain to mention some. As in the previous sections, in order to understand the nature of the time dependence of the scattered intensity we must understand the dynamics of the objects that scatter light. The polymer dynamics at different concentration regimes or in constrained systems such as permanent gels is beyond the scope of this chapter; the reader interested in this field can consult a classical modern treatise on the subject such as Doi and Edwards' [75] or de Gennes' books [76]. In any case, in what follows, we illustrate the main results as far as DLS is concerned, from the single chain (dilute solutions) to cooperative diffusion process at higher concentrations and other diffusion processes that occur in polymers with a microstructure, such as block copolymers.

Let us consider a dilute polymer solution of flexible macromolecules. The dynamics of a single Gaussian chain has been around for many years in the context of the molecular theory of transport phenomena in polymer solutions and has been fully reviewed in textbooks or articles in this subject [77]. Rouse's theory is about the simplest of all them and helps understand the basic ingredients of the theory [78]. Rouse proposed a simplification of the problem by representing a polymer chain as a collection of beads connected by springs (the bead and spring model). The solvent interacts with the chain through the beads and it is assumed to freely drain through the chain. The only interaction between the beads is through the springs. The spring constant will be given as an effective entropic elastic constant produced by a collection of monomers whose end-to-end distance is the bead size b, that is, $k = 3k_BT/b^2$. The total friction exerted by the fluid on the chain is $\zeta_R = N\zeta$, where N is the number of beads and ζ is the friction coefficient of each bead. Since the model is already a coarse-grained picture of the chain, it can only give a reasonable answer for the slow long "wavelength" motions. In summary, the Rouse model reduces the problem to the dynamics of Brownian motion of coupled oscillators. The solution to the dynamics problem is well known and can be expressed as a superposition of normal modes.[5] The correlation function of these modes decays exponentially with time, and the relaxation time of the p-mode is given by

$$\tau_p = \frac{\tau_1}{p^2} \quad \text{for} \quad p = 1, 2 \ldots \tag{18.82}$$

where

$$\tau_1 \cong \frac{\zeta N^2 b^2}{3\pi^2 k_B T} \tag{18.83}$$

[5]A normal mode is an independent collective motion. The equation that describes the dynamics of a normal mode is not coupled to the other modes. A general motion of the chain can be written as a superposition of its normal modes.

The zero mode is the self-diffusion of the center of mass whose diffusion coefficient is given by the Stokes–Einstein relation $D = k_BT/N\zeta$. The time τ_1 will be proportional to the time required for a chain to diffuse an end-to-end distance, that is, $\approx \langle R^2\rangle/D = \zeta N^2 b^2/k_BT$. This means that for time scales longer than τ_1 the motion of the chain will be purely diffusive. On timescales shorter than τ_1, it will exhibit viscoelastic modes. However, the dynamics of a single chain in a dilute solution is more complex due to long-range forces; hydrodynamic interactions between distant monomers through the solvent are present and, in good solvents, excluded volume interactions also have to be taken into account. The correction of the Rouse model for hydrodynamic interaction was done by Zimm [79]. From a mathematical point of view, the problem becomes harder and requires approximations to arrive at some useful results. In this case, the translational diffusion coefficient obtained is

$$D \approx \left(\frac{k_BT}{\eta b}\right) N^{-\nu} \approx \frac{k_BT}{\eta R_g} \tag{18.84}$$

where ν in good solvents is close to 3/5 and in θ-solvents is 1/2. The relaxation time of mode p is

$$\tau_p = \tau_1 p^{-3\nu} \tag{18.85}$$

where

$$\tau_1 \cong \frac{\eta \langle R^2\rangle^{3/2}}{k_BT} \cong \frac{\eta b^3}{k_BT} N^{3\nu} \tag{18.86}$$

which is close to the experimentally observed molecular weight dependence for D and τ_1 in both θ-solvents and good solvents. If we compare the Rouse models with those of Zimm for θ-solvents, we see that while in the former, D and τ_1 scale with M as $D \approx M^{-1}$ and $\tau_1 \approx M^2$ and in Zimm's theory D and τ_1 scale as $D \approx M^{-1/2}$ and $\tau_1 \approx M^{3/2}$. From these results, we can conclude that the Rouse chain suffers a larger frictional force than the corresponding Zimm chain. In fact, according to Equation 18.84, the chain moves as a solid sphere of radius R_g, which means that the chain is dragging the solvent within the chain, whereas in the Rouse model, the chain is fully free draining and all the beads suffer the same friction.

Pecora analyzed $g_1(\mathbf{q}, t)$ for the Rouse model and found that this could be written in the form

$$g_1(\mathbf{q}, t) \approx S_0\left(q^2R_g^2\right) \exp\left(-q^2Dt\right) + S_2\left(q^2R_g^2\right) \exp\left[-\left(q^2D + \frac{2}{t_1}\right)\right] + \cdots \tag{18.87}$$

He arrived at the conclusion that for small qR_g values, the first term was fully dominant and only the

diffusion of the center of mass (D) could be observed [80]. However, for $qR_g \geq 1.73$, the first relaxation time starts to influence $g_1(\mathbf{q}, t)$. A simple calculation tells us that in order to observe the first internal relaxation mode, the polymer chain must have an extremely high molecular weight. In fact, most dynamic light experiments in the dilute regime that tried to observe the first internal relaxation mode were performed with very high molecular polymers on the order of several million Daltons [81, 82]. In the intermediate q region defined as $qR_g \gg 1$ but $q\ell < 1$ where ℓ is an effective monomer length, Dubois-Violette and de Gennes [83] showed that $g_1(\mathbf{q}, t)$ scaled as $g_1(\mathbf{q}, t) \approx \exp\left(f\left[\omega_c(q)t\right]\right)$ where $\omega_c(q)t$ is a dimensionless time. They obtained explicitly the form of f for the case of an unperturbed Gaussian chain and found that $\omega_c(q) \approx (k_B T/\eta)q^3$. Akcasu and Benmouna [84] obtained the first cumulant $\langle\Gamma(q)\rangle$ for all q regions, including the transition zone, for different models of chain and without preaveraging the hydrodynamic interactions. They found, in the intermediate region, the same scaling law for $\omega_c(q)$ than Dubois-Violette and de Gennes. For $qR_g \ll 1$, they recovered the usual diffusive behavior. Lodge et al. (82b) confirmed experimentally this scaling law in the intermediate q region in a temperature range going from θ-solvent to a good solvent. However, the authors found a small and systematic deviation of the experimentally found $\langle\Gamma(q)\rangle$ with that predicted by Akcasu and Bemouna without preaveraging approximation. Recently Li et al. (82c) found experimentally that for temperatures below the θ temperature, this scaling law no longer holds.

As the concentration increases and reaches the local concentration of a single chain c^*, the chains start to overlap each other. The limiting concentration c^* can vary depending on solvent quality and temperature. Concentration higher than c^* but lower than the entanglement concentration c_e is called the *semidilute regime*. When $c > c_e$, we refer it as a *concentrated solution*. When $c > c_e$, all chains entangle with each other. Each chain could be visualized as being for a short time within a tube made of the surrounding chains and whose diameter depends on concentration. In fact, at a particular instant we can picture the entangled mesh, with an average mesh size ξ (the correlation length) and therefore the tube diameter will be on the order of ξ and will only depend on concentration. In an athermal solvent, a portion with average size ξ (blob) of the chain inside the tube will not interact with other chains. So we can imagine the chain inside the tube as formed of a collection of blobs of g monomers each. Since the first cumulant in only related to the short time dynamics, the motion that we will be concerned at high concentrations is that produced by the thermally excited monomers inside the blobs that will concomitantly produce Brownian motion of their center of mass.

At higher concentrations, besides a fast mode (cooperative diffusion), other modes are present by DLS even for lower molecular weight polymers, since other cooperative phenomena occur that involve more chains or aggregates of these.

Recently, Li et al. [85] reexamined the slow relaxation mode and found that in dust-free samples of monodisperse PS, the solvent quality was a definitive factor in observing or not observing the slow mode. For athermal solvents for PS such as benzene, they showed that even at concentrations as high as 20% only one fast diffusive mode was observed (Fig. 18.15a). In contrast, they showed that the slow mode for c > c * is enhanced as the solvent quality decreases. In cyclohexane, in which solvent quality for PS decreases when temperature decreases from 50 to 32 °C, they observed a slow mode, in addition to the cooperative diffusion (fast mode). In Figure 18.15b, $G_2(\mathbf{q}, t)$ shows a single fast mode for a PS with $M_w = 1.83 \times 10^6$ Da in cyclohexane at 50 °C for $c/c^* \approx 1$; however, when $c/c^* > 1$, a second mode appears. All samples in this study were prepared in the same way, except the solvent used and the concentration. Cyclohexane is a good solvent of PS at 50 °C, but it is not athermal. They concluded that if c is only a few times larger than the overlap concentration (c^*) but lower than the entanglement concentration (c_e), the slow mode is related to transient interchain segment–segment interaction induced clusters. Actually, for $c/c^* = 1.4$, they were able to observe the slow mode with molecular weights as low as 4.6×10^{-4} Da; reinforcing their conclusion was the fact that this mode was more notorious at *small angles*. For $c > c_e$, it is attributed to the confinement of each chain inside an inhomogenous tube with a "band"-like structure due to relatively stronger segment–segment interaction near the entanglement points.

In fact, having all chains entangled with each other they form a large cluster and, at short times, only the blobs can jiggle around in the tube; their motion will depend on how close they are to an entanglement point. In contrast with the semidilute regime, for $c > c_e$, the slow mode is most pronounced when observed *at large angles*, implying that it is not related to the scattering of some large object. They also pointed out that in the athermal solvent, there is no interaction between the chain blobs and the tube so that they experience the same microenvironment resulting in only a diffusive relaxation mode. Finally, in their study, the scaling law of $\langle\Gamma\rangle_{slow}$ with q depended on the concentration, going from q^3 for dilute solutions to q^0 at high concentrations, suggesting that the origin of the slow mode is different for each concentration regime.

Following the same line of thought, Yuan et al. [86] applied DLS to thermally responsive systems such as poly(N-isopropylacrilamide) (PNIPAM) or poly(ethylene oxide)-b-poly(propylene oxide)-b-poly(ethylene oxide) (PEO-PPO-PEO) in water. Similar to the PS/cyclohexane

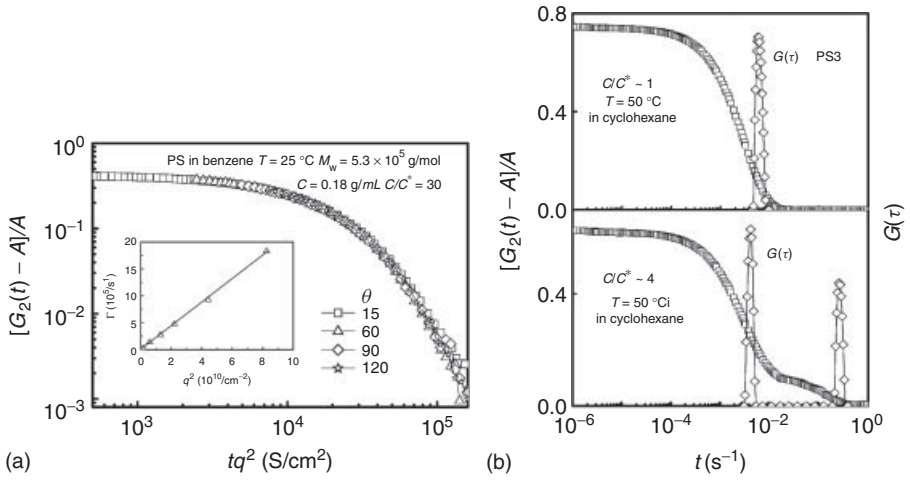

Figure 18.15 Intensity–intensity time correlation function for a solution of PS in benzene and cyclohexane. (a) A highly concentrated athermal solution of PS in benzene: only a single diffusive mode is present. The inset shows the q^2 dependence of $\langle\Gamma\rangle$. (b) $G_2(\mathbf{q}, t)$ and the distribution of time relaxation ($G(\tau)$) for a solution of a 1.83×10^6 PS in cyclohexane at 50 °C at concentrations $c \approx c^*$ and $c \approx 4\ c^*$. *Source*: Reprinted with permission from Li J, Li W, Huo H, Luo S, Wu C. *Macromolecules* 2008;41:901 [85]. Copyright 2008 American Chemical Society.

system, they were able to use the temperature dependence of the solvent–polymer interaction in both systems to investigate the temperature-induced shrinkage of polymer chains. The difference in nature of the slow mode in these two systems is that as the solvent becomes poorer, PNIPAM/H_2O aggregates, whereas PEO-PPO-PEO/H_2O forms micelles.

Another interesting application of DLS is the work by Pan et al. [87] on the dynamics of block copolymers in the vicinity of an order–disorder transition (ODT). Motivated by the phenomena encountered near the ODT, such as chain stretching and large amplitude concentration fluctuations, Pan et al. studied the polymer dynamics of solutions of symmetric block copolymers of poly(styrene-*b*-isoprene) (PSI) from dilute, semidilute, and concentrated regimes. Previously, Benmouna and coworkers [88] had predicted two dynamical modes: a cooperative diffusion, with a diffusion coefficient D_C (C-mode) corresponding to the relaxation of fluctuations in polymer concentration, and an internal mode (Γ_I), reflecting relative motion of the centers of mass of the two blocks on a single chain. Semenov et al. [89], in addition, predicted a third mode: the heterogeneity mode (H-mode) due to chain-to-chain fluctuations in composition and that relaxes by translational diffusion with a diffusion coefficient D_H. They assumed that these modes are uncoupled, and therefore, $g_1(\mathbf{q}, t)$ can be written as a sum of exponentials. The decay constants for the cooperative diffusion and heterogeneity mode are of the form q^2D, given their diffusive character, as we shall see, whereas the internal mode has a decay constant $\Gamma_I \approx \tau_1^{-1}$, where τ_1 is the longest viscoelastic relaxation time of the chain.

In semidilute and concentrated solutions, D_C and D_H are cleanly resolved; however, in these concentration regimes, the internal mode Γ_I was only observed in the higher molecular weight blocks used in the study (3.4×10^5 Da and referred to as SI(170-170) with a number fraction of 0.5 for the PS block). In all the systems used in this study, $qR_g < 1$. In the semidilute regime, they confirmed that D_C scaled with concentration as $\approx c^{0.70}$, independent of the molecular weight (M). It was also observed that translational diffusivity was unaffected by the ODT. The relative amplitudes of D_C and D_H also scaled with c, M, and the refractive index of the solvent, n_s, as predicted by the theory. Figure 18.16a shows a representative intensity correlation function at 90° for the SI(170-170) copolymer at various weight fractions (w). For this block copolymer, the limiting concentration c^* between the dilute and semidilute regimes corresponds to $w = 0.0169$. Using the Siegert relation to obtain $g_1(\mathbf{q}, t)$ and CONTIN to perform the Laplace inversion, they resolved the modes' contribution to $g_1(\mathbf{q}, t)$, as shown in Figure 18.16b. In dilute solutions, as expected, only one diffusive mode is present and is attributed to a superposition of D_C and D_H. As we reach the semidilute regime, the H- and C-modes are clearly resolved, with the C-mode being dominant. As we increase the concentration furthermore ($w = 0.049$), an intermediate mode appears, which was assigned to the internal mode, and the contribution of H-mode overpasses that of the C-mode as predicted by the theory. At higher concentrations only the H-mode is well resolved; this data correspond to a solution close to the ordered state. As stated above, the Laplace inversion methods do not give us a high resolution $G(\Gamma)$,

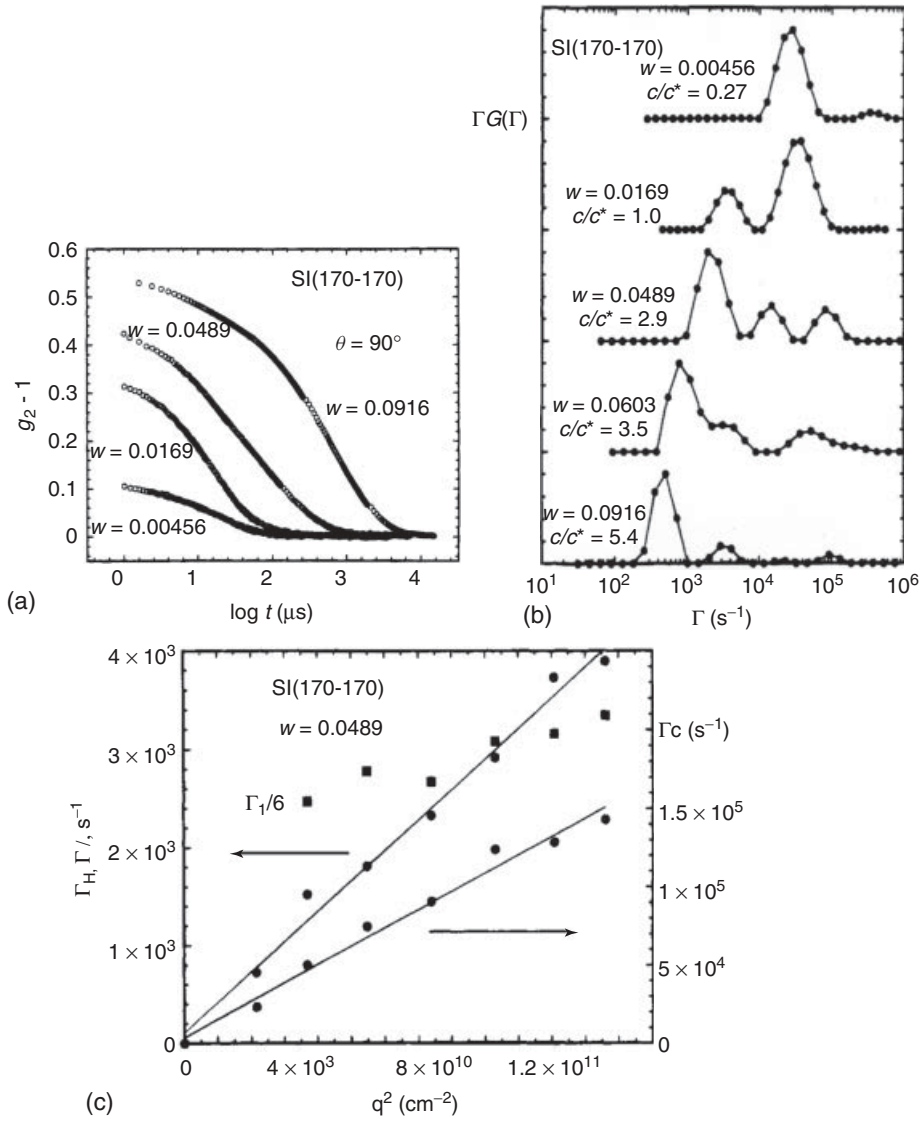

Figure 18.16 Intensity–intensity correlation functions for a symmetric PS-PI block copolymer with $M_w = 3.4 \times 10^5$ Da in benzene at different weight concentrations. (a) $G_2(q, t)$ versus w; (b) the Laplace inversion time decay rate distribution $G(\Gamma)$; (c) Γ versus $\mathbf{q}^2$ for the three modes. *Source*: Reprinted with permission from Pan C, Maurer W, Liu Z, Lodge TP, Stepanek P, von Meerwall ED, Watanabe H. *Macromolecules* 1995;28:1643 [87]. Copyright 1995 American Chemical Society.

and if two modes are not well separated, as is the case with Γ_I and Γ_C, then they might appear as a single mode; this is even worse if one of the modes has comparatively a smaller contribution to $G(\Gamma)$ such as Γ_I. Finally, Figure 18.16c shows the q^2 dependence of Γ_H and Γ_C, proving their diffusive character, whereas Γ_I has a mild q dependence for $qR_g < 0.5$.

The study of internal modes by DLS has led to many interesting applications, for example, the effect of crosslinking on dynamics during sol–gel transition [90], the study of the apparent diffusion coefficient on hyperbranched starch samples [55], structural relaxation in glassy polymers [91], diffusion in concentrated colloidal suspensions and glasses [92], and many more that we cannot review in this chapter because of space constraints.

REFERENCES

1. [a] Maret G, Wolf PE. Z Phys B 1987;65:409. [b] Pine DJ, Weitz DA, Chaikin PM, Herbolzheimer E. Phys Rev Lett 1988;60:1134. [c] Weitz DA, Pine DJ. Diffusing-wave spectroscopy. In: Brown W, editor. *Dynamic Light Scattering*.

New York: Oxford University Press; 1993. p 652. [d] Scheffold F, Romer S, Cardinaux F, Bissig H, Stradner A, Rojas-Ochoa LF, Trappe V, Urban C, Skipetrov SE, Cipelletti L, Schurtenberger P. Progr Colloid Polymer Sci 2004;123:141.

2. [a] Brown RGW. Appl Opt 1987;26:4846. [b] Wiese H, Horn D. J Chem Phys 1991;94:6429. [c] Auweter H, Horn D. J Colloid Interface Sci 1985;105:399.
3. [a] Phillies GDJ. Phys Rev A 1981;24:1939. [b] Schätzel K. J Mod Opt 1991;38:1849. [c] Segrè PN, Van Megen W, Pusey PN, Schätzel K, Peters W. J Mod Opt 1995;42:1929. [d] Stieber F, Richtering W. Langmuir 1995;11:4724.
4. [a] Aberle LB, Hulstede P, Wiegand S, Schroer W, Staude W. Appl Opt 1998;37:6511. [b] Urban C, Schurtenberger P. J Colloid Interface Sci 1998;207:150. [c] Pusey PN. Curr Opin Colloid Interface Sci 1999;4:177. [d] Block I, Scheffold F. Rev Sci Instrum 2010;81:123107.
5. van de Hulst HC. *Light Scattering by Small Particles*. New York: John Wiley; 1957.
6. [a] Kerker M. *The Scattering of Light and Other Electromagnetic Radiation*. New York: Academic Press; 1969. [b] Bohren C, Huffman D. *Absorption and Scattering of Light by Small Particles*. New York: John Wiley; 1983.
7. Mishchenko MI, Travis LD, Lacis AA. *Scattering, Absorption, and Emission of Light by Small Particles*. Cambridge: Cambridge University Press; 2002.
8. Landau LD, Lifshitz EM, Pitaevskii LP. *Electrodynamics of Continuous Media*. 2nd ed. Vol. 8. Oxford, UK: Butterworth-Heinemann; 1984.
9. [a] Lord Rayleigh (Strutt JW), Philos Mag 1871;41:107. [b] Lord Rayleigh (Strutt JW), Philos Mag 1881;12:81.
10. Glatter O, Kratky O, editors. *Small Angle X-ray Scattering*. New York: Academic Press; 1982.
11. [a]Lovesey SW. *The Theory of Neutron Scattering from Condensed Matter*. Vol. 1 & 2. Oxford: Oxford University Press; 1984. [b] Hammouda B. J Macromol Sci Polymer Rev 2010;50:14.
12. von Smoluchowski M. Ann Phys 1908;25:205.
13. Einstein A. Ann Phys 1910;33:1275.
14. Brinkman HC, Hermans JJ. J Chem Phys 1949;17:574.
15. Stockmayer WH. J Chem Phys 1950;18:58.
16. Kirkwood JG, Goldberg RJ. J Chem Phys 1950;18:54.
17. Strazielle C. Light Scattering in Mixed Solvents In: Huglin MB, editor. *Light Scattering by Polymer Solutions*. London: Academic Press; 1972. p 633.
18. Stockmayer WH, Moore LD Jr,, Fixman M, Epstein BN. J Polym Sci 1955;16:517.
19. Bushuk W, Benoit H. Can J Chem 1958;36:1616.
20. Benoit H and Froelich D. Application of Light Scattering to Copolymers In: Huglin MB, editor. *Light Scattering by Polymer Solutions*. London: Academic Press; 1972. p 467.
21. Casassa EF, Eisenberg H. J Phys Chem 1960;64:753.
22. Casassa EF, Eisenberg H. J Phys Chem 1961;65:427.
23. Tuzar Z, Kratochvil P, Straková D. Eur Polym J 1970;6:1113.
24. Tuzar Z, Kratochvil P. Colin Czech Chem Commun 1967;32:3358.
25. Podešva J, Stejskal J, Kratochvíl P. Macromolecules 1987;20:2195.
26. Read BE. Trans Faraday Soc 1960;56:382.
27. Vrij A, Overbeek JTG. J Colloid Sci 1962;17:570.
28. [a] Strazielle C, Benoit H. J Chim Phys 1961;58:675. [b] Strazielle C, Benoit H. J Chim Phys 1961;58:678.
29. Lange H. Makromol Chem 1965;86:192.
30. Stockmayer WH, Chan L-L. J Polym Sci A 1966;4:437.
31. Mauss Y, Chambron J, Daune M, Benoit H. J Mol Biol 1967;27:579.
32. Marchal E, Strazielle C. Compt Rendu 1968;C267:135.
33. Cowie JMG. Pure Appl Chem 1970;23:355.
34. Zimm BH. J Chem Phys 1948;16:1093.
35. Debye P. Ann Phys 1915;46:809.
36. Debye P. J Phys Colloid Chem 1947;51:18.
37. Debye P, Anacker EW. J Phys Colloid Chem 1951;55:644.
38. Zimm BH. J Chem Phys 1948;16:1099.
39. Chu B, Wu C. Macromolecules 1987;20:93.
40. Kratochvíl P. Particle Scattering Functions In: Huglin MB, editor. *Light Scattering by Polymer Solutions*. London: Academic Press; 1972. p 333.
41. [a]Burchard W. Adv Polym Sci 1983;48:1. [b] Burchard W. Adv Polym Sci 1999;143:113.
42. [a]Benoit H. J Polymer Sci 1953;11:507. [b]Benoit H, Holtzer AM, Doty P. J Phys Chem 1954;58:635.
43. Holtzer A. J Polymer Sci 1955;17:432.
44. Galinsky G, Burchard W. Macromolecules 1997;30:4445.
45. Burchard W. Macromolecules 1977;10:919.
46. Dobashi T, Narita T, Masuda J, Makino K, Mogi T, Ohshima H, Takenaka M, Chu B. Langmuir 1998;14:745.
47. Lonetti B, Tsigkri A, Lang PR, Stellbrink J, Willner L, Kohlbrecher J, Lettinga MP. Macromolecules 2011;44:3583.
48. Kholodenko AI. Macromolecules 1993;26:4179.
49. Schärtl W. *Light Scattering from Polymer Solutions and Nanoparticle Dispersions*. Berlin, Heidelberg: Springer-Verlag; 2007.
50. Berne BJ, Pecora R. *Dynamic Light Scattering*. New York: John Wiley & Sons; 1976.
51. Siegert AJF, Massachusetts Institute of Technology, Boston, MA. 1943. M.I.T. Rad. Lab. Rep., No. 465.
52. Ford NC. Theory and practice of photon correlation spectroscopy. In: Dahneke BE, editor. *Measurement of Suspended Particles by Quasi-elastic Light Scattering*. New York: Wiley-Interscience; 1983. p 31.
53. [a] McWhirter JG, Pike ER. J Phys A Math Gen 1978;11:1729. [b] McWhirter JG. Opt Acta 1980;27:8.
54. Koppel DE. J Chem Phys 1972;57:4814.
55. Galinsky G, Burchard W. Macromolecules 1997;30:6966.
56. Ostrowsky N, Sornett D, Parker P, Pike ER. Opt Acta 1981;28:1059.

57. Provencher SW, Hendrix J, De Maeyer L, Paulussen N. Chem Phys 1978;69:4273.
58. [a] Provencher SW. Makromol Chem 1979;180:201. [b] Bryant G, Abeynayake C, Thomas J. Langmuir 1996;12:6224.
59. Gull SF. Developments in maximum entropy data analysis. In: Skilling J, editor. *Maximum Entropy and Bayesian Methods*. Dordrecht: Kluwer Academic Publishers; 1989. p 53–71.
60. Jakes J. Czech J Phys 1988;38:1305.
61. De Vos C, Deriemaeker L, Finsy R. Langmuir 1996;12:2630.
62. Finsy R. Adv Colloid Interface Sci 1994;52:79.
63. Bryant G, Thomas J. Langmuir 1995;11:2480.
64. [a] Vega JR, Gugliotta LM, Gonzalez VDG, Meira GR. J Colloid Interface Sci 2003;261:74. [b] Gonzalez VDG, Gugliotta LM, Vega JR, Meira GR. J Colloid Interface Sci 2005;285:581. [c] Gugliotta LM, Stegmayer GS, Clementi LA, Gonzalez VDG, Minari RJ, Leiza JR, Vega JR. Part Part Syst Char 2009;26:41.
65. Clementi LA, Vega JR, Gugliotta LM, Orlande HRB. Chemometr Intell Lab Syst 2011;107:165.
66. Pecora R. J Chem Phys 1964;40:1604.
67. Pecora R. J Chem Phys 1968;48:4126.
68. Doi M, Edwards SF. *The Theory of Polymer Dynamics*. Oxford: Clarendon Press; 1988. Chapter 8.
69. Wilcoxon J, Schurr JM. Biopolymers 1983;22:849.
70. Maeda T, Fujime S. Macromolecules 1984;17:1157.
71. Hammouda B. Macromolecules 1985;18:293.
72. [a] Broersma S. J Chem Phys 1960;32:1626. [b] Broersma S. J Chem Phys 1981;74:6989. [c] Tirado MM, García de la Torre J. J Chem Phys 1979;71:2581. [d] Tirado MM, García de la Torre J. J Chem Phys 1986;1980:73. [e] Tirado MM, López Martínez C, García de la Torre J. J Chem Phys 1984;81:2047.
73. Buitenhuis J, Dhont JKG, Lekkerkerker HNW. J Colloid Interface Sci 1994;162:19.
74. Lehner D, Lindner H, Glatter O. Langmuir 2000;16:1689.
75. Doi M, Edwards SF. *The Theory of Polymer Dynamics*. Oxford: Clarendon Press; 1988.
76. de Gennes PG. *Scaling Concepts in Polymer Physics*. Ithaca, NY: Cornell University Press; 1979.
77. [a] Yamakawa H. *Modern Theory of Polymer Solutions*. New York: Harper & Row; 1971. Chapter 6. [b] Doi M, Edwards SF. *The Theory of Polymer Dynamics*. Oxford: Clarendon Press; 1988. Chapter 4. [c] Stockmayer WH. Dynamics of chain molecules. In: Balian R, Weill G, editors. *Molecular Fluids*. New York: Gordon and Breach; 1976.
78. Rouse PEJ. J Chem Phys 1953;21:1272.
79. Zimm BH. J Chem Phys 1956;24:269.
80. Pecora R. J Chem Phys 1968;49:1032.
81. Huang WN, Frederick JE. Macromolecules 1974;7:34.
82. [a] Han CC, Akcasu AZ. Macromolecules 1981;14:1080. [b] Lodge TP, Han CC, Akcasu AZ. Macromolecules 1983;16:1180. [c] Li J, Lu Y, Zhang G, Wu C. Chin J Polym Sci 2008;26:775.
83. Dubois-Violette E, de Gennes PG. Physics 1967;3:181.
84. Akcasu AZ, Benmouna M, Han CC. Polymer 1980;21:866.
85. Li J, Li W, Huo H, Luo S, Wu C. Macromolecules 2008;41:901.
86. Yuan G, Wang X, Han CC, Wu C. Macromolecules 2006;39:3642.
87. Pan C, Maurer W, Liu Z, Lodge TP, Stepanek P, von Meerwall ED, Watanabe H. Macromolecules 1995;28:1643.
88. [a] Benmouna M, Duval M, Borsali R. J Polym Sci Polym Phys Ed 1987;25:1839. [b] Benmouna M, Benoit H, Borsali R, Duval M. Macromolecules 1987;20:2620.
89. Semenov AN, Fytas G, Anastasiadis SH. Polymer Prepr 1994;35:618.
90. [a] Ngai T, Wu C, Chen Y. J Phys Chem B 2004;108:5532. [b] Ngai T, Wu C, Chen Y. Macromolecules 2004;37:987. [c] Ngai T, Wu C. Macromolecules 2003;36:848. [d] Li J, Ngai T, Wu C. Polym J 2010;42:609.
91. [a] Patterson GD. Adv Polym Sci 1983;48:125. [b] Forrest JA, Svanbera C, Revesz K, Rodahl M, Torell LM, Kasemo B. Phys Rev E 1998;58:R1226.
92. [a] Bartsch E. Curr Opin Colloid Interface Sci 1998;3:577. [b] Cipelletti L, Weeks ER. Glassy dynamics and dynamical heterogeneity in colloids. In: Berthier L, Biroli G, Bouchaud J-P, Cipelletti L, editors. *Dynamical Heterogeneities in Glasses, Colloids, and Granular Media*. Oxford, UK: Oxford University Press; 2011.